Non-linear seismic analysis of RC shear wall

Participation in OECD/NEA seismic shear wall international standard problem on Japanese seismic ultimate response test

Jagd, Lars

Publication date:
1997

Document Version
Publisher's PDF, also known as Version of record

Institut for Bærende Konstruktioner og Materialer
Department of Structural Engineering and Materials
Danmarks Tekniske Universitet • Technical University of Denmark

BKM

Non-linear Seismic Analysis of RC Shear Wall

Participation in OECD/NEA Seismic Shear Wall International Standard Problem on Japanese Seismic Ultimate Response Test

Lars Kristian Jagd

Serie R No 5 1996

Non-linear Seismic Analysis of RC Shear Wall

Tryk:
LTT
Danmarks Tekniske Universitet
Lyngby
ISBN 87-7740-173-5
ISSN 1396-2167
Bogbinder:
H. Meyer, Bygning 101, DTU

Non-linear Seismic Analysis of RC Shear Wall

Participation in OECD/NEA Seismic Shear Wall International Standard Problem on Japanese Seismic Ultimate Response Test

Lars Kristian Jagd

PREFACE

This report has been prepared as one part of the thesis required to obtain the Ph.D. degree at the Technical University of Denmark.

The work has been carried out at the Department of Structural Engineering and Materials under the supervision of professor, dr.techn. M.P.Nielsen.

I wish to thank my supervisor for his advice and encouragement during the whole process. Also I wish to thank the entire staff at the department for their help during the time I have been here.

Financial assistance from the Danish Council for Scientific and Technical Research (STVF) is gratefully acknowledged.

Lyngby, 1996

Lars Kristian Jagd

ABSTRACT

In 1991, the Nuclear Power Engineering Corporation (NUPEC) in Japan performed dynamic tests until failure of two reinforced concrete shear walls using the largest high-performance shaking table in the world. NUPEC has offered OECD's Nuclear Energy Agency (NEA) the test data as an open International Standard Problem with the purpose of verifying seismic response analysis methods. This report contains the analyses and results from the Danish contribution.

The analyses consist of a static non-linear FEM analysis of the shear wall followed by non-linear dynamic analyses of a lumped mass single degree of freedom model of the structure.

The static analysis has been performed by a non-linear FEM programme that is being developed at present. The programme takes into account the non-linear material behaviour of concrete, rotating crack directions, sliding in old cracks and compressive strength reduction effects.

The non-linear load/displacement relationship found in the static analysis is used as envelope curve in the dynamic analyses. Hysteresis features that include stiffness degradation and pinching effects are used to describe the cyclic behaviour of the shear wall. The trapezoidal rule combined with Newton/Raphson iterations have been used to solve the initial value problem.

The CPU time for the static analysis is about 15 minutes, the CPU time for all the dynamic analyses about 15 seconds (586/100 MHz PC with 8MB RAM). The results compare quite well with the actual test results.

TABLE OF CONTENTS

0.0 INTRODUCTION

0.1 General

Seismic design of reinforced concrete structures is a matter of great concern. Still today, earthquakes are responsible for the loss of large human and economic resources. For this reason, research aiming at a better understanding of the behaviour of structures subjected to dynamic loading is necessary.

Especially in the case of nuclear installations, understanding and prediction of the dynamic behaviour of structures and of the equipment and piping within these, are important factors.

Since 1986, the Nuclear Power Engineering Corporation (NUPEC) in Japan has conducted large tests in order to improve and develop seismic analysis codes and to enhance reliability of seismic safety evaluation methods. As part of these projects tests were performed in 1991 with the purpose of studying the dynamic response characteristics of reinforced concrete shear walls as major earthquake resisting elements of a reactor building. One of the primary goals was to obtain experimental data to verify seismic response analysis methods, ref. [94.1].

These tests were some of the largest dynamic tests until failure of reinforced concrete specimens ever made. The weight of the specimens was about 200 tons. The vibration tests were done in Tadotsu Engineering Laboratory using the largest high-performance shaking table in the world, ref. [94.1].

NUPEC has offered OECD's Nuclear Energy Agency the test data as an open International Standard Problem (ISP). The proposal for the ISP was sent out in March 1994, and this report contains the result from the Danish contribution. The layout of this report is in accordance with the specification given in [94.2]. This chapter contains general information regarding the ISP.

0.2 The International Standard Problem

The geometry of the test specimen can be seen in figure 0.1.

The weight of the top slab is 29.1 tons. At the top slab, additional weights of 92.9 tons are present. These weights are fixed at the upper and lower surface of the top slab, resp. The total weight of the top slab, including the additional weights, is 122.0 tons.

The reinforcement in the web wall is D6@70 bars (deformed bars, nominal diameter 6.35 mm, spacing 70 mm) in each side of the wall both horizontally and vertically. D6@175 bars are used for the vertical reinforcement of the flange walls. As an exception, D6@70 bars are used for the vertical reinforcement at the intersections of the web wall and the flange walls.

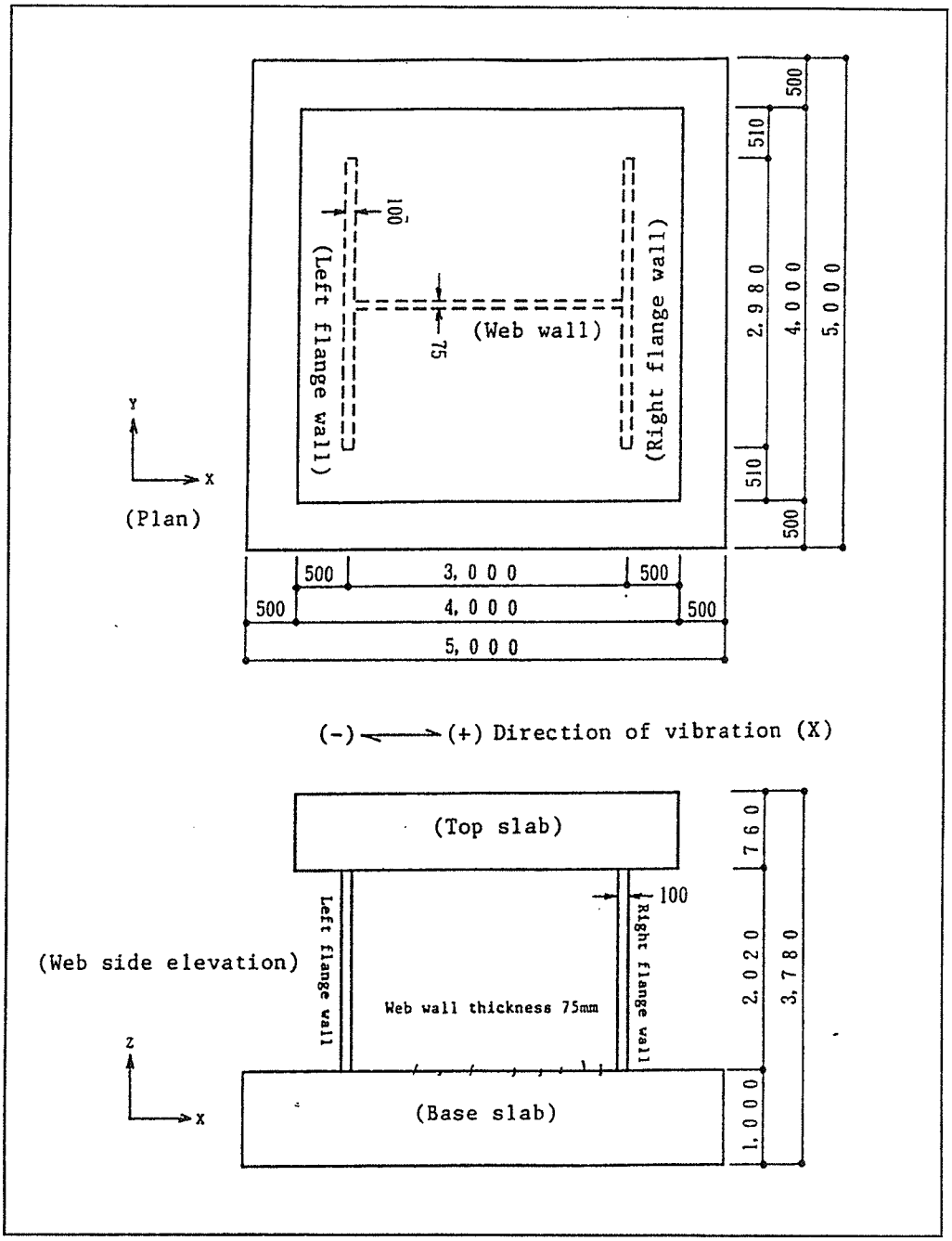

Figure 0.1: The test specimen, ref. [94.2] (measurements in mm).

For detailed information about geometry, additional weights, reinforcement and concrete, see ref. [94.2].

The structure was subjected to 6 vibration steps of increasing magnitude (named RUN1, RUN2, RUN2', RUN3, RUN4 and RUN5). The shear wall failed during RUN5. The duration of the prepared input wave was 10 seconds. The horizontal accelerations at the top of the base slab (the input accelerations) can be seen in appendix A.

The maximum acceleration measured at the top of the base slab, in each of the 5 runs, can be seen in table 0.1:

RUN number:	Maximum acceleration (m/s^2)
1	0.530
2	1.120
2'	3.040
3	3.520
4	5.044
5	12.300

Table 0.1: Maximum acceleration at top of base slab.

0.3 Short Description of Analysis Method

The results in this report are based on a static non-linear FEM analysis of the shear wall followed by a non-linear dynamic analysis of a lumped mass single degree of freedom system. The non-linear FEM programme used is being developed at present at the Department of Structural Engineering, Technical University of Denmark, ref. /96.1/.

1.0 GENERAL INFORMATION

1.1 Computer Information

Type of Computer:

Personal Computer (PC), 586/100 MHz

Memory Size:

8 MB RAM

1.2 Code Information

Category of Analytical Method:

Non-linear dynamic analysis by means of a single degree of freedom lumped-mass model based on the results of a non-linear static FEM analysis.

Code Name and Version:

The computer code used is original.

Total Number of Degrees of Freedom:

In the static FEM analysis, the total number of Degrees of Freedom (DOF's) is 420. The number of nodes is 210 (2 DOF's per node), and the number of elements used is 182 (4 nodes per element). The element mesh and a description of the type of element used may be found in section 2. In the dynamic lumped mass analysis 1 DOF is present.

Non-linear Analysis Algorithm:

The load/displacement curve found in the non-linear static analysis has been determined by applying constant horizontal displacement increments at the top slab. The stiffnesses in each load step are determined by the constitutive laws of the concrete and the reinforcement, as described in section 3.

Due to the large concentration of masses at the top slab, it has been considered reasonable to base the dynamic analyses on a single degree of freedom model. The mass of the top slab including the additional weights has been lumped into one mass. This mass is then supported by a spring and allowed to move in the horizontal direction only. The spring stiffness is given by the load/displacement curve determined in the non-linear static analysis and a set of hysteresis rules, see section 2.5.

The trapezoidal rule has been used for the time integration scheme, see e.g. [82.1]. For each time step Δt, an iteration method using the modified Newton-Raphson method is used to obtain equilibrium. The mass and damping properties are kept constant during each RUN. The governing equilibrium equation at the time $t+\Delta t$, iteration k is given by **(1.1)**:

$$
\begin{aligned}
Ma_k^{t+\Delta t} + Cv_k^{t+\Delta t} + K^t \Delta u_k &= R^{t+\Delta t} - F_{k-1}^{t+\Delta t} \\
u_k^{t+\Delta t} &= u_{k-1}^{t+\Delta t} + \Delta u_k
\end{aligned}
\tag{1.1}
$$

The sup-/subscripts denote the corresponding time/iteration number. u, v and a are the displacements, velocities and accelerations, resp. M, C and K are the mass, damping and stiffness coefficients, resp. R is the externally applied load, and F is the nodal point force.

Using the trapezoidal rule of time integration, the displacement increment at iteration k can be found by **(1.2)**:

$$
\begin{aligned}
&\left[K^t + \frac{4}{\Delta t^2}M + \frac{2}{\Delta t}C\right]\Delta u_k = \\
&\quad R^{t+\Delta t} - F_{k-1}^{t+\Delta t} - M\left[\frac{4}{\Delta t^2}\left(u_{k-1}^{t+\Delta t} - u^t\right) - \frac{4}{\Delta t}v^t - a^t\right] - C\left[\frac{2}{\Delta t}\left(u_{k-1}^{t+\Delta t} - u^t\right) - v^t\right]
\end{aligned}
\tag{1.2}
$$

For each time step, the initial conditions **(1.3)** are used:

$$
\begin{aligned}
u_0^{t+\Delta t} &= u^t \\
F_0^{t+\Delta t} &= F^t
\end{aligned}
\tag{1.3}
$$

When the displacement increment is below a given residual value, the iteration process is stopped, and the new velocities and accelerations are found by **(1.4)**:

$$
\begin{aligned}
a^{t+\Delta t} &= \frac{4}{\Delta t^2}\left[u^{t+\Delta t} - u^t\right] - \frac{4}{\Delta t}v^t - a^t \\
v^{t+\Delta t} &= v^t + \frac{\Delta t}{2}\left[a^{t+\Delta t} + a^t\right]
\end{aligned}
\tag{1.4}
$$

1.3 Dynamic Analysis Condition

In table 1.1, the applied time step, the CPU time for 12 seconds of analysis and whether or not vertical input is taken into account is stated for each run.

Run	1	2	3	4	5
Time Step (s)	0.001	0.001	0.001	0.001	0.001
CPU time (s)	3	3	3	3	3
Vert. input	No	No	No	No	No

Table 1.1: Dynamic analysis general information.

1.4 Static Analysis Condition

A constant displacement increment of 1/10 mm was used at the top slab. A total of 166 load steps, corresponding to a total displacement of 16.6 mm, were applied.

The CPU time of the static analysis was 988 sec.

2 MODEL DESCRIPTION

2.1 Element Mesh Scheme

In figure 2.1 the element mesh is shown. All elements used are HOTCH-POTCH disk elements, see section 2.2.

The model is two-dimensional. The flange walls have been modelled as disk elements with thicknesses corresponding to the length of the flange wall (2980 mm), while the web wall has been modelled by disk elements with thicknesses corresponding to the actual thickness of the web wall (75 mm). The base slab has not been modelled. The top slab has been modelled by very stiff disk elements.

The gravity forces from the top slab and the additional masses have been applied as initial loads at the top of the structure. The gravity forces from the masses in the shear wall have been neglected.

The shear wall is supported rigidly at the base.

2.2 Element Type Used

The element used is the so-called 'HOTCH-POTCH' Disk Element, ref. [94.3]. This element is based on a simple, mechanical model, that causes normal stresses to be concentrated in stringers along the element edges, and shear to be transferred by a constant in-plane shear stress field. The element has a transparent behaviour very similar to the stringer method, and the constant shear stress within each element makes it well-suited for analysis and design

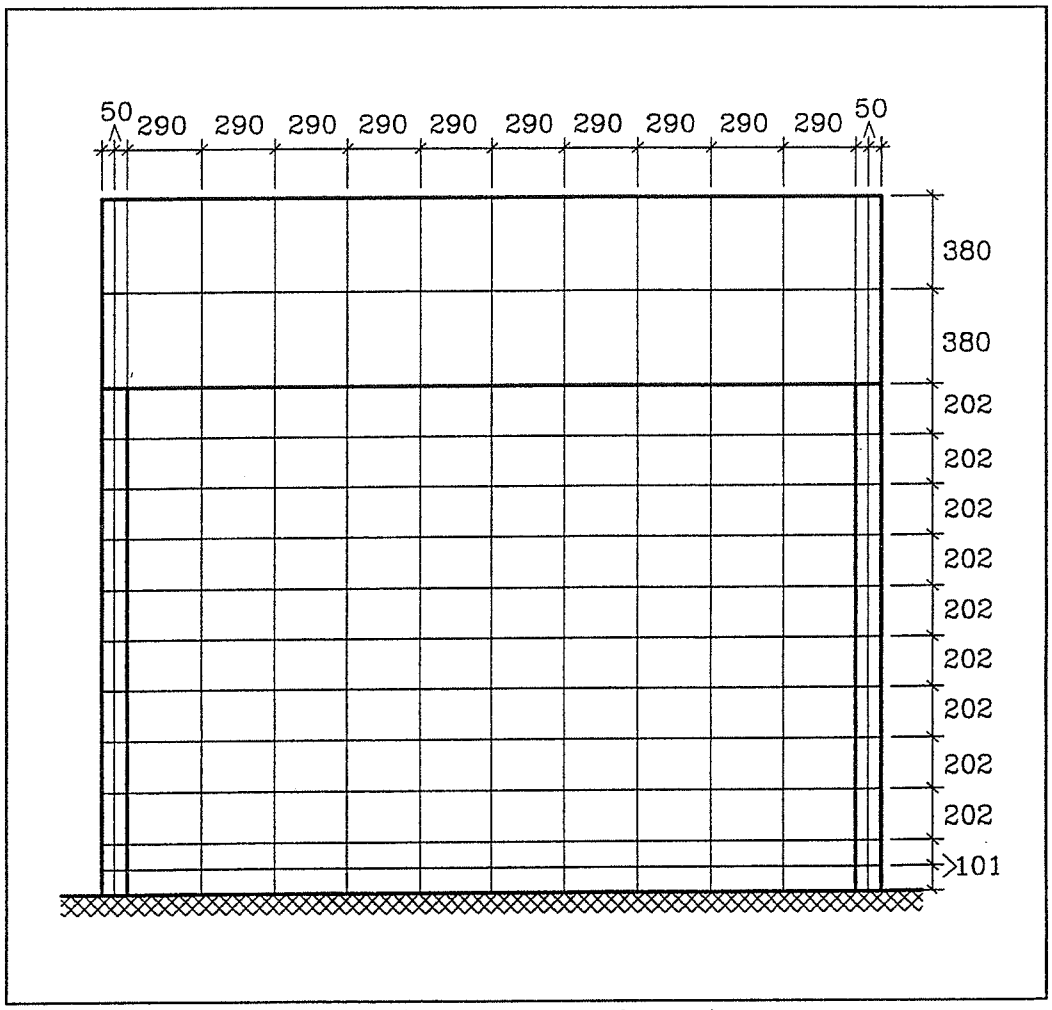

Figure 2.1: Element mesh (measurements in mm).

of reinforced concrete disks. The element is neither a compatible nor an equilibrium element and is therefore called the 'HOTCH-POTCH' disk element.

The element has four nodes and is rectangular with side lengths l_1 and l_2, see figure 2.2. In each of the four stringers, the reinforcement ratio ρ may be specified. The number of freedom degrees in each node is 2 (displacement u in x- and y-direction, resp).

The normal stiffnesses are concentrated in stringers along the four edges of the element. Contributions are present from the concrete as well as the reinforcement. The normal stiffness k of the stringer from node 1 to node 2 is given by **(2.1)**:

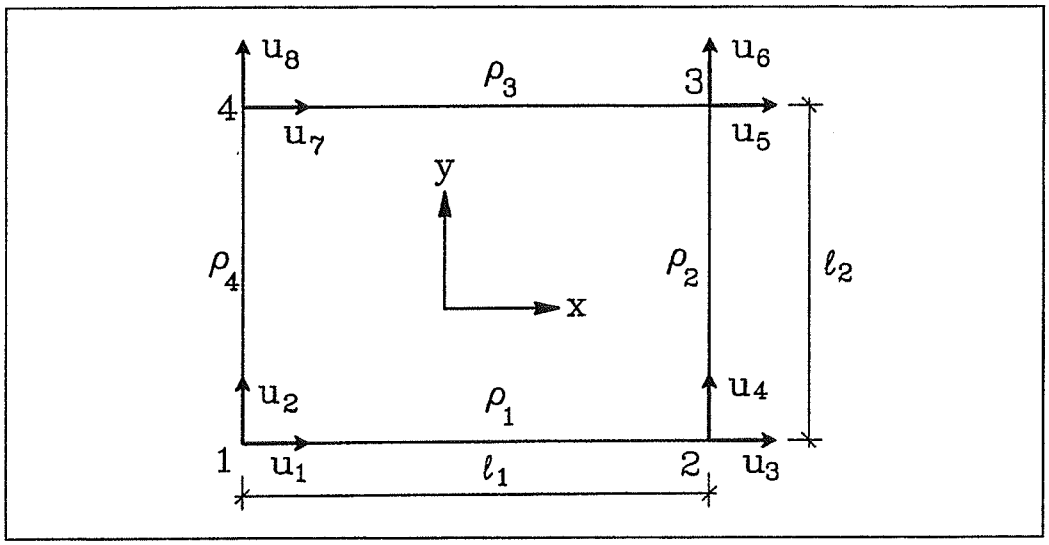

Figure 2.2: The HOTCH-POTCH disk element.

$$k = E_s \cdot \rho \cdot \frac{l_2}{2} \cdot \frac{1}{l_1} + E_c \cdot t \cdot \frac{l_2}{2} \cdot \frac{1}{l_1} \qquad \textbf{(2.1)}$$

E_s and E_c is Young's Modulus of reinforcement and of concrete, resp.

The shear strain within the element is assumed to be constant and calculated from the mean displacements in each stringer. As the reinforcement is parallel to the element edges, only the concrete contributes to the shear stiffness.

The element stiffness matrix $\underline{k}$ is given by **(2.2-3)**:

$$\underline{k} = \begin{bmatrix} k_1+k_5 & k_7 & -k_1+k_5 & -k_7 & -k_5 & -k_7 & -k_5 & k_7 \\ k_7 & k_4+k_6 & k_7 & -k_6 & -k_7 & -k_6 & -k_7 & -k_4+k_6 \\ -k_1+k_5 & k_7 & k_1+k_5 & -k_7 & -k_5 & -k_7 & -k_5 & k_7 \\ -k_7 & -k_6 & -k_7 & k_2+k_6 & k_7 & -k_2+k_6 & k_7 & -k_6 \\ -k_5 & -k_7 & -k_5 & k_7 & k_3+k_5 & k_7 & -k_3+k_5 & -k_7 \\ -k_7 & -k_6 & -k_7 & -k_2+k_6 & k_7 & k_2+k_6 & k_7 & -k_6 \\ -k_5 & -k_7 & -k_5 & k_7 & -k_3+k_5 & k_7 & k_3+k_5 & -k_7 \\ k_7 & -k_4+k_6 & k_7 & -k_6 & -k_7 & -k_6 & -k_7 & k_4+k_6 \end{bmatrix} \qquad \textbf{(2.2)}$$

$$
\begin{aligned}
k_1 &= \frac{1}{2}\cdot(E_s\cdot \rho_1 + E_c\cdot t)\cdot\frac{l_2}{l_1} \\
k_2 &= \frac{1}{2}\cdot(E_s\cdot \rho_2 + E_c\cdot t)\cdot\frac{l_1}{l_2} \\
k_3 &= \frac{1}{2}\cdot(E_s\cdot \rho_3 + E_c\cdot t)\cdot\frac{l_2}{l_1} \\
k_4 &= \frac{1}{2}\cdot(E_s\cdot \rho_4 + E_c\cdot t)\cdot\frac{l_1}{l_2} \\
k_5 &= \frac{1}{4}\cdot G\cdot t\cdot\frac{l_1}{l_2} \\
k_6 &= \frac{1}{4}\cdot G\cdot t\cdot\frac{l_2}{l_1} \\
k_7 &= \frac{1}{4}\cdot G\cdot t
\end{aligned}
\qquad (2.3)
$$

Here G is the shear modulus of the concrete.

2.3 Spring Model Scheme

The entire model is lumped into one mass M (weight 122 ton, corresponding to weight of top slab and additional weights). Only displacements in the horizontal direction are possible. Total motions are denoted by subscript t. Support motions are denoted by subscript g. The spring model scheme is shown in figure 2.3.

The equilibrium of the system is given by **(2.4)**:

$$Ma_t + Cv + Ku = 0 \qquad (2.4)$$

This can be written as **(2.5)**, ref. [75.1]:

$$Ma + Cv + Ku = -Ma_g(t) \qquad (2.5)$$

For each time step, by applying a load corresponding to the mass M multiplied by the input acceleration at the base slab at this time, the numerical method described in section 1 will yield displacements, velocities and accelerations relative to the ground.

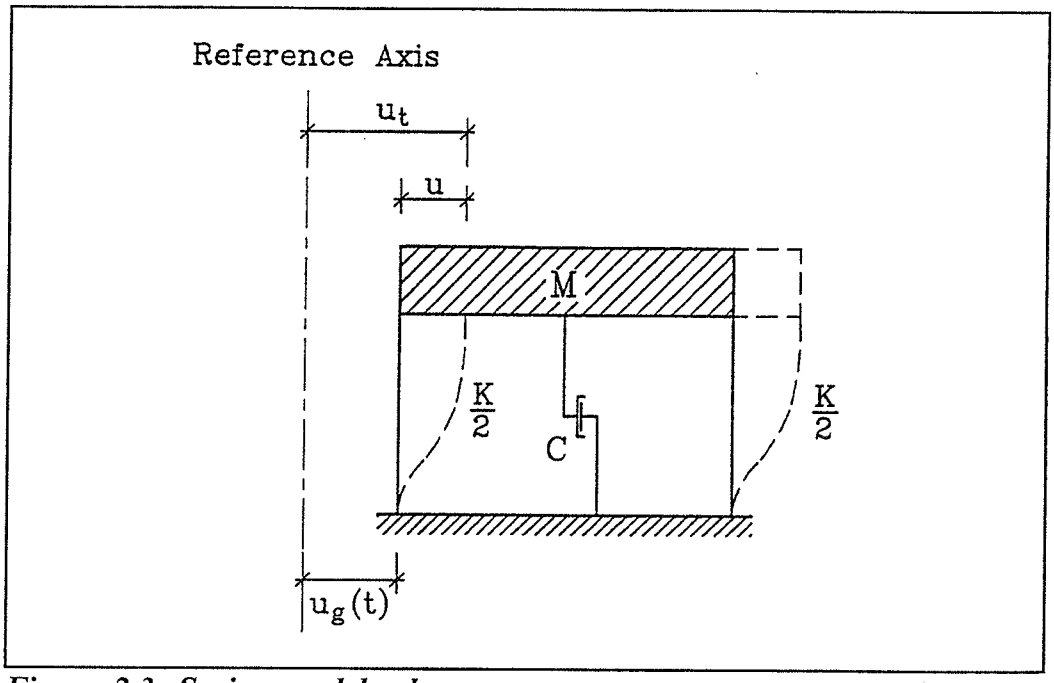

Figure 2.3: Spring model scheme.

2.4 Stiffness Evaluation of Spring

The stiffness of the spring is defined by the load/displacement curve found in the non-linear static FEM-analysis, see figure 2.4.

The expressions **(2.6)** found by using best fit methods are used to analytically represent the load/displacement curve in the dynamic programme:

$$\begin{aligned} -16.3mm \le u < -0.8mm: \quad & F = -0.555\cdot10^6N + 156.6\cdot10^6N/m\cdot u + \\ & \quad 4{,}598\cdot10^6N/m^2\cdot u^2 \\ |u| \le 0.8mm: \quad & F = 846.5\cdot10^6N/m\cdot u \\ 0.8mm < u \le 16.3mm: \quad & F = 0.555\cdot10^6N + 156.6\cdot10^6N/m\cdot u - \\ & \quad 4{,}598\cdot10^6N/m^2\cdot u^2 \end{aligned} \qquad (2.6)$$

The specimen is considered to have failed if absolute displacements larger than 16.3 mm occur.

In figure 2.4, the actual results from the FEM-analysis have been shown with a full line while the expressions **(2.6)** have been shown with a dotted line.

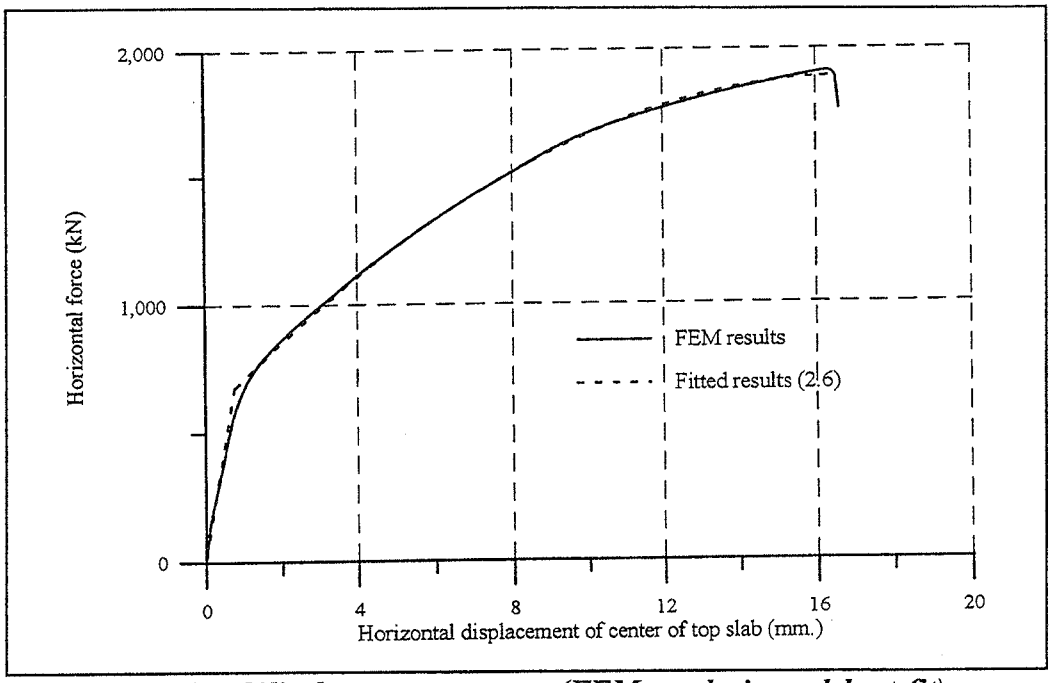

Figure 2.4: Load/displacement curves (FEM analysis and best-fit).

2.5 Hysteresis Loop of Spring

The applied hysteresis behaviour is illustrated in figure 2.5.

For each element, the maximum response points, during the whole loading history, are stored (including preceding RUN's). For positive displacements/-positive displacement increments and for negative displacements/negative displacement increments, the reloading branches of the hysteresis loops are directed at these previous maximum response points. Otherwise, in order to model pinching action, the reloading branches are directed at the points P_p/-P_p on the vertical axis. The unloading slope is similar to the original slope K_0.

A value of P_p=80,000 N has been used in these analyses.

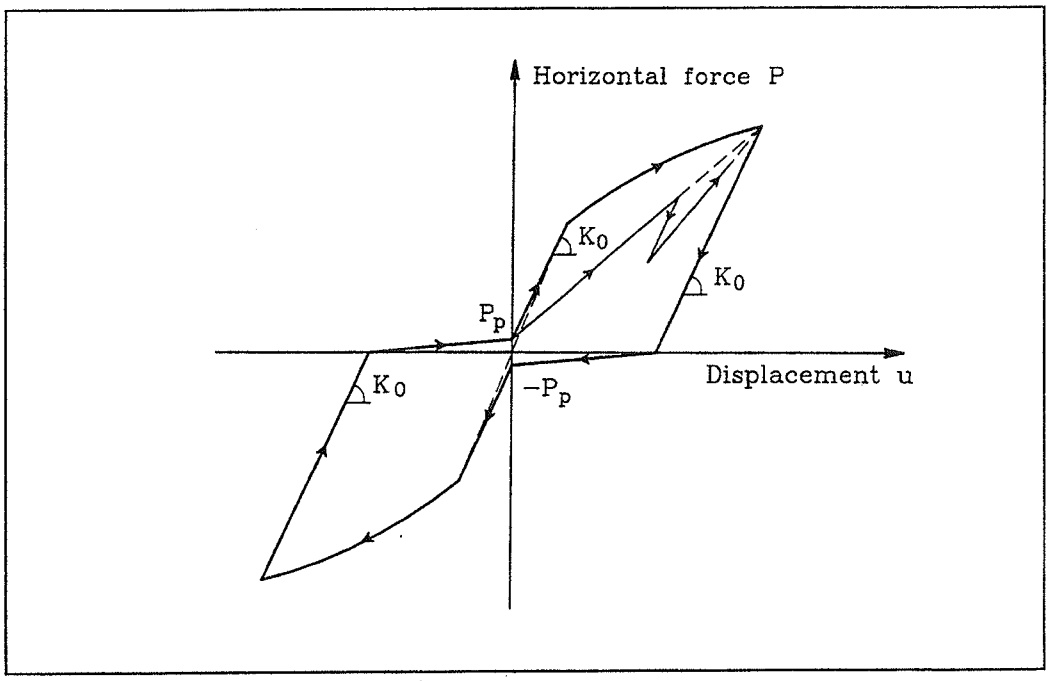

Figure 2.5: Hysteresis behavior.

2.6 Evaluation of Damping

The damping ratios in table 2.1 have been applied to the single DOF system as viscous damping.

RUN:	Damping Ratio:
1	1%
2	1%
3	2%
4	2%
5	2%

Table 2.1: Applied damping ratios.

In RUN1 and RUN2, elastic behaviour is expected and thus no hysteresis damping will be present. For these RUNs, a viscous damping of 1% has been considered reasonable. For RUN3-5, non-linear behaviour is significant and this will introduce hysteresis damping on top of the viscous damping.

3 CONSTITUTIVE LAW OF CONCRETE

3.1 General

A detailed description of the constitutive models used can be found in ref. [96.1]. In this chapter, the main features of the models are described.

A smeared crack model is used. When uncracked, the orthotropic stiffnesses of the HOTCH-POTCH disk element are determined by the principal strains and the uniaxial stress/strain relationship.

When the maximum tensile stress exceeds the tensile strength of the concrete, the element cracks. After cracking, the orthotropic stiffnesses are determined by the strains parallel to and perpendicular to the crack, resp. The shear stiffness in the crack is kept at a high level. This makes is possible for shear stresses to build up in the crack surface. Additional cracks will occur in the element each time the tensile stress in another section exceeds the tensile strength of the concrete.

If the shear stress in a crack surface exceeds the maximum allowable shear stress, determined by a modified Coulomb yield criteria, sliding occurs in the crack. In this case, the stiffnesses of the element are determined by elasto-plastic constitutive relationships.

3.2 Stress/strain Diagram

Compressive stresses/strains are defined as positive.

If uncracked, the orthotropic stiffnesses of the HOTCH-POTCH disk element are determined by the two principal strains defining the principal strain coordinate system $x'y'$, see figure 3.1.

If cracks are present in an element, the normal stiffnesses are determined by the normal strains in the coordinate system defined by the newest crack. The coordinate system $x'y'$ is now defined by the crack direction.

In plane stress, the generalized Hooke's law is given by **(3.1)**.

$$\begin{pmatrix} \sigma_{x'} \\ \sigma_{y'} \\ \tau_{x'y'} \end{pmatrix} = \begin{bmatrix} Q_{11} & Q_{12} & 0 \\ Q_{12} & Q_{22} & 0 \\ 0 & 0 & Q_{66} \end{bmatrix} \begin{pmatrix} \epsilon_{x'} \\ \epsilon_{y'} \\ \gamma_{x'y'} \end{pmatrix} \tag{3.1}$$

where $\underline{\sigma}$ are the stresses, Q_{11}, Q_{12}, Q_{22} and Q_{66} are the components of the stiffness matrix and $\underline{\epsilon}$ the engineering strains.

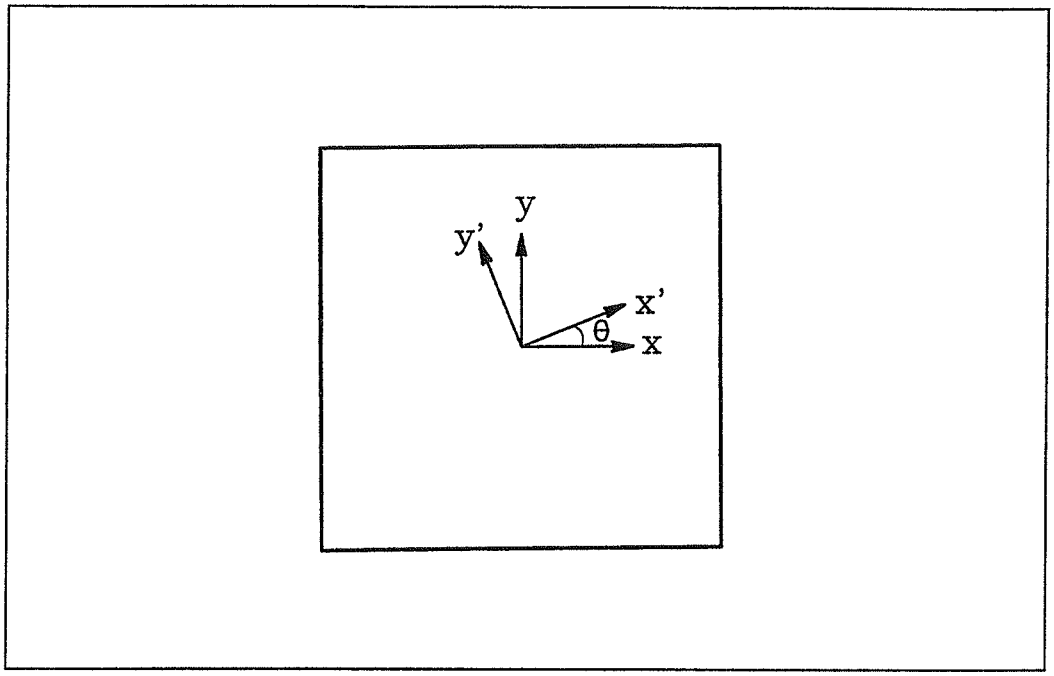

Figure 3.1: Definition of coordinate systems.

If not cracked, the normal stiffnesses Q_{11} and Q_{22} are determined as functions of the normal strains in the $x'y'$-system from the uniaxial stress/strain relationship in figure 3.2.

If cracked, the normal stiffnesses Q_{11} and Q_{22} are determined as functions of the normal strains in the $x'y'$-system from the uniaxial stress/strain relationship in figure 3.3. A similar behaviour for non-crushed/crushed concrete is used.

The material parameters for the concrete used in this analysis can be seen in table 3.1:

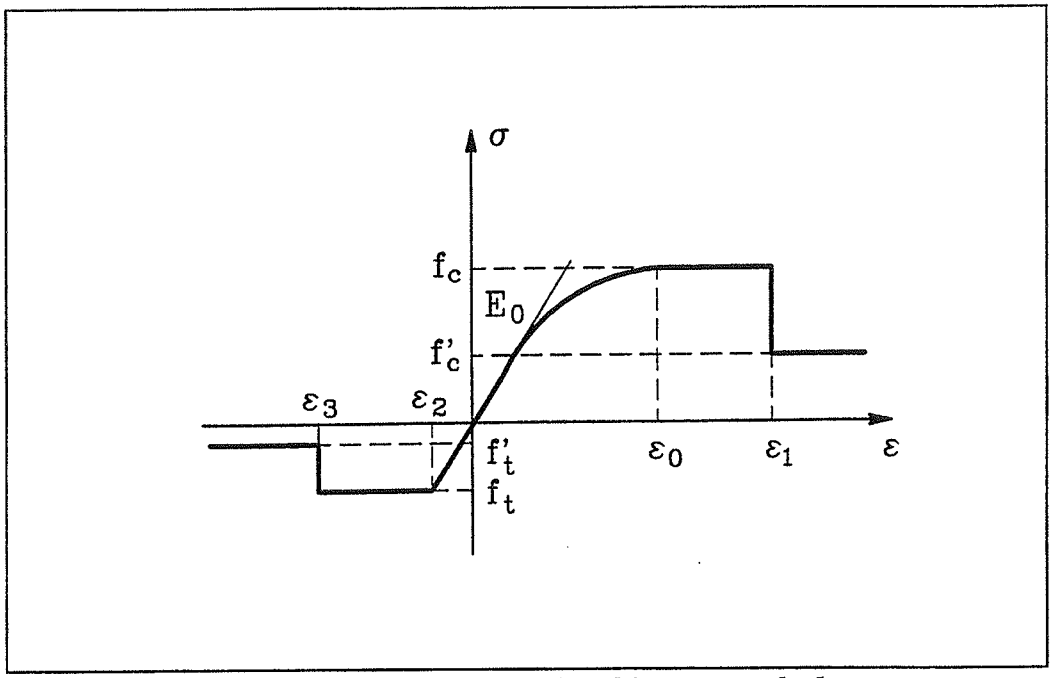

Figure 3.2: Uniaxial stress/strain relationship, uncracked concrete.

f_c	28.64 MPa
f_c'	0 MPa
f_t	-1.5 MPa
f_t'	0 MPa
E_0	22.95 GPa
ϵ_0	0.0027
ϵ_1	0.0050
ϵ_2	0.000065
ϵ_3	0.000157
ν	0.15/0.00
η	2400 kg/m^3

Table 3.1: Material parameters used.

ν is the Poisson's ratio which is taken as 0.15 if uncracked and 0.00 if cracked.
η is the density of the combined concrete/reinforcement.

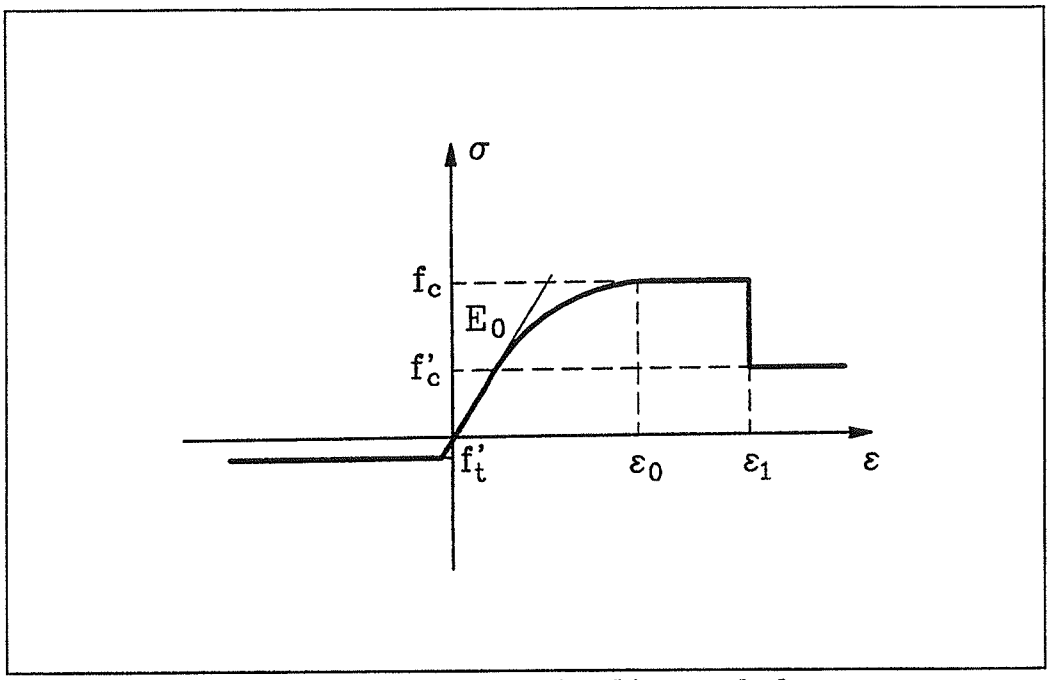

Figure 3.3: Uniaxial stress/strain relationship, cracked concrete.

The stress/strain relationship in the compressive range from $\epsilon=0$ to $\epsilon=0.0027$ is given by the following expression suggested in [92.1] **(3.2)**:

$$\sigma = f_c\left[1 - \left(1-\frac{\epsilon}{\epsilon_0}\right)^n\right] \qquad \textbf{(3.2)}$$

where:

$$n = \frac{E_0\,\epsilon_0}{f_c} \qquad \textbf{(3.3)}$$

The initial value of Young's Modulus E_0 has been calculated as a function of f_c by the following expression, also suggested in [92.1] (f_c in MPa):

$$E_0 = 10{,}300 f_c^{0.3} \quad (f_c \text{ in } MPa) \tag{3.4}$$

The shear stiffness Q_{66} is determined as half the average value of the two normal stiffnesses.

The constitutive equations in the *xy*-system are given by **(3.5)**, ref. [80.1]:

$$\begin{pmatrix} \sigma_x \\ \sigma_y \\ \tau_{xy} \end{pmatrix} = \begin{bmatrix} \overline{Q}_{11} & \overline{Q}_{12} & \overline{Q}_{16} \\ \overline{Q}_{12} & \overline{Q}_{22} & \overline{Q}_{26} \\ \overline{Q}_{16} & \overline{Q}_{26} & \overline{Q}_{66} \end{bmatrix} \begin{pmatrix} \epsilon_x \\ \epsilon_y \\ \gamma_{xy} \end{pmatrix} \tag{3.5}$$

where:

$$\begin{aligned}
\overline{Q}_{11} &= Q_{11}\cos^4\theta + Q_{22}\sin^4\theta + 2(Q_{12} + 2Q_{66})\sin^2\theta\cos^2\theta \\
\overline{Q}_{22} &= Q_{11}\sin^4\theta + Q_{22}\cos^4\theta + 2(Q_{12} + 2Q_{66})\sin^2\theta\cos^2\theta \\
\overline{Q}_{12} &= (Q_{11} + Q_{22} - 4Q_{66})\sin^2\theta\cos^2\theta + Q_{12}(\cos^4\theta + \sin^4\theta) \\
\overline{Q}_{66} &= (Q_{11} + Q_{22} - 2Q_{12} - 2Q_{66})\sin^2\theta\cos^2\theta + Q_{66}(\sin^4\theta + \cos^4\theta) \\
\overline{Q}_{16} &= (Q_{11} - Q_{12} - 2Q_{66})\cos^3\theta\sin\theta - (Q_{22} - Q_{12} - 2Q_{66})\cos\theta\sin^3\theta \\
\overline{Q}_{26} &= (Q_{11} - Q_{12} - 2Q_{66})\cos\theta\sin^3\theta - (Q_{22} - Q_{12} - 2Q_{66})\cos^3\theta\sin\theta
\end{aligned} \tag{3.6}$$

Assuming a constant value of θ, the incremental constitutive equations are given by **(3.7)**:

$$\begin{pmatrix} \Delta\sigma_x \\ \Delta\sigma_y \\ \Delta\tau_{xy} \end{pmatrix} = \begin{bmatrix} Q_{11} & Q_{12} & Q_{16} \\ Q_{12} & Q_{22} & Q_{26} \\ Q_{16} & Q_{26} & Q_{66} \end{bmatrix} \begin{pmatrix} \Delta\epsilon_x \\ \Delta\epsilon_y \\ \Delta\gamma_{xy} \end{pmatrix} \tag{3.7}$$

3.3 Compressive Strength Reduction

When a crack is formed in reinforced concrete, the rebars near the cracks will cause a slip followed by punching of the concrete. This is illustrated in figure 3.4 taken from Y.Goto, ref. [71.1].

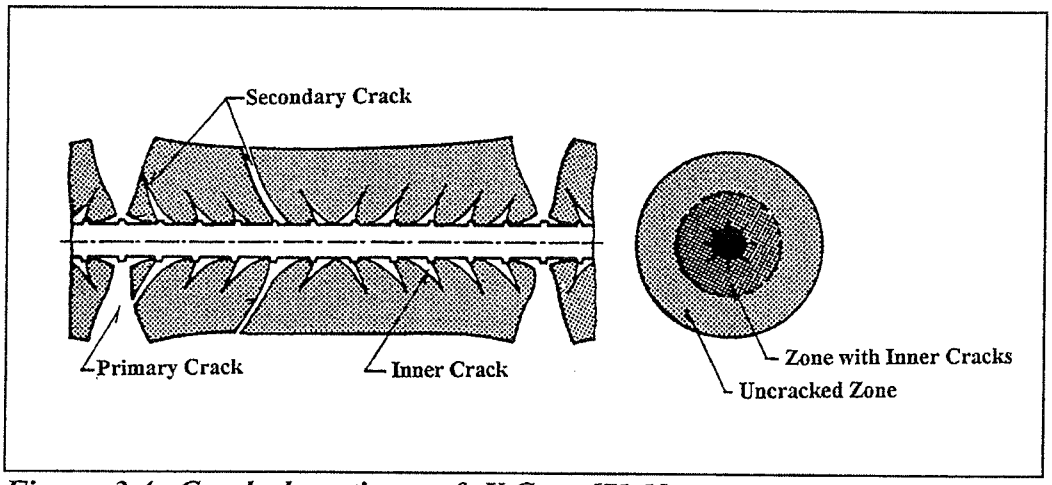

Figure 3.4: Cracked section, ref. Y.Goto [71.1].

Goto examined cracking in concrete by injecting ink into round test specimens and subjecting these to pure tension. The punching and the internal cracking around the rebar will cause a reduction in the compressive strength parallel to the crack. Based on these observations, it is considered reasonable to determine a reduced compressive strength as a function of the tensile stresses perpendicular to the crack surface.

The reduced compressive strength f_c^r is expressed as an effectiveness factor ν multiplied by the compressive strength f_c, **(3.8)**:

$$f_c^r = \nu f_c \tag{3.8}$$

The value of the effectiveness factor ν can be determined by figure 3.5, ref. /96.1/. The term X is given by **(3.9)**:

$$X = \frac{\rho \sigma_s}{1.43\sqrt{f_c}} \tag{3.9}$$

ρ is the reinforcement ratio and σ_s the reinforcement stress. The reinforcement direction causing the largest reduction is used.

As can be seen, the proposed reduction is a function of the compressive strength of the concrete and the tensile stress. In the case of plain concrete, the reduction will be zero.

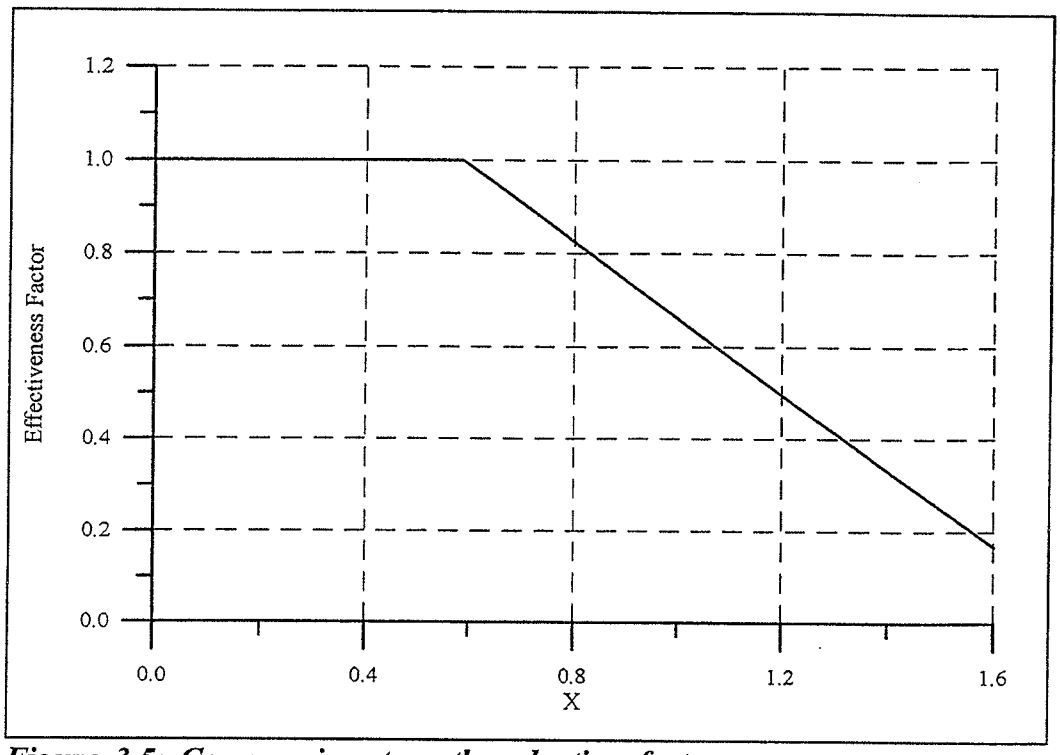

Figure 3.5: Compressive strength reduction factor.

3.4 Cracking and Crushing

A crack is introduced when one of the principal stresses become lower (numerically larger) than the tensile strength f_t. The stress level in the element is decreased to the level f_t', and a force equivalent to this change in stress level is applied to the system. This may in turn generate new cracks.

Crushing is handled similarly.

3.5 Yield Model

If the shear stress in a crack reaches the maximum shear stress given by the yield condition shown in figure 3.6, plastic sliding occurs. The plastic strain increments ϵ and γ (normal strain and change of angle, resp.) are given by the normality condition. The angle between the plastic strain vector and the vertical axis is referred to as α.

According to the theory of plasticity, ref. [84.1] c, the cohesion, is given by **(3.10)**:

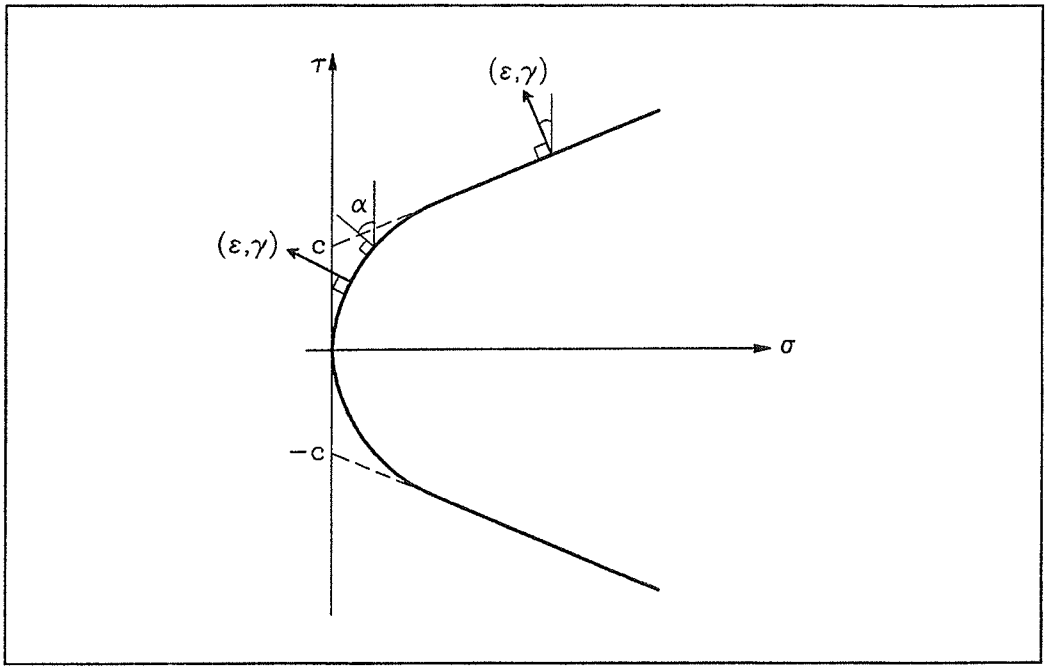

Figure 3.6: Dissipation in yield line (crack surface).

$$c = \frac{1}{4}\nu f_c \tag{3.10}$$

where ν is an effectiveness factor. Recent studies at the Department of Structural Engineering at the Technical University of Denmark, ref. [94.4], show, that for cracked concrete this effectiveness factor can be expressed as

$$\nu = \nu_s \nu_0 \tag{3.11}$$

where ν_s is the effectiveness factor for uncracked concrete, and ν_s is the sliding reduction factor due to cracking. The angle of friction is taken as 37 degrees.

The following values for ν_0 and ν_s taken from [84.1] and [94.4], resp., are used **(3.12)**:

$$\nu_0 = 0.7 - \frac{f_c}{200}, \quad (f_c \text{ in } MPa) \qquad \textbf{(3.12)}$$
$$\nu_s = 0.5$$

For reasons of simplicity, hardening/softening behaviour has been neglected in this investigation. Thus, when yielding, the stress/strain relationship in the crack coordinate system $x'y'$ is given by the elastoplastic constitutive equations **(3.13-14)**.

$$\begin{pmatrix} \sigma_x' \\ \sigma_y' \\ \tau_{x'y'} \end{pmatrix} = \begin{bmatrix} Q_{11}Q_{66}k & 0 & \tan^2\alpha Q_{11}Q_{66}k \\ 0 & Q_{22} & 0 \\ \tan^2\alpha Q_{11}Q_{66}k & 0 & \tan\alpha Q_{11}Q_{66}k \end{bmatrix} \begin{pmatrix} \epsilon_{x'} \\ \epsilon_{y'} \\ \gamma_{x'y'} \end{pmatrix} \qquad \textbf{(3.13)}$$

where:

$$k = \frac{1}{\tan^2\alpha Q_{11} + Q_{66}} \qquad \textbf{(3.14)}$$

4.0 CONSTITUTIVE LAW OF REBAR

The stress/strain diagram used for the rebars is depicted in figure 4.1:

The material parameters used for the rebars have been taken from [94.2], see table 4.1:

E_s	184.37 GPa
E_s'	0.353 GPa
ϵ_y	0.00208
ϵ_u	0.291
σ_y	383 MPa

Table 4.1: Material parameters used for rebars.

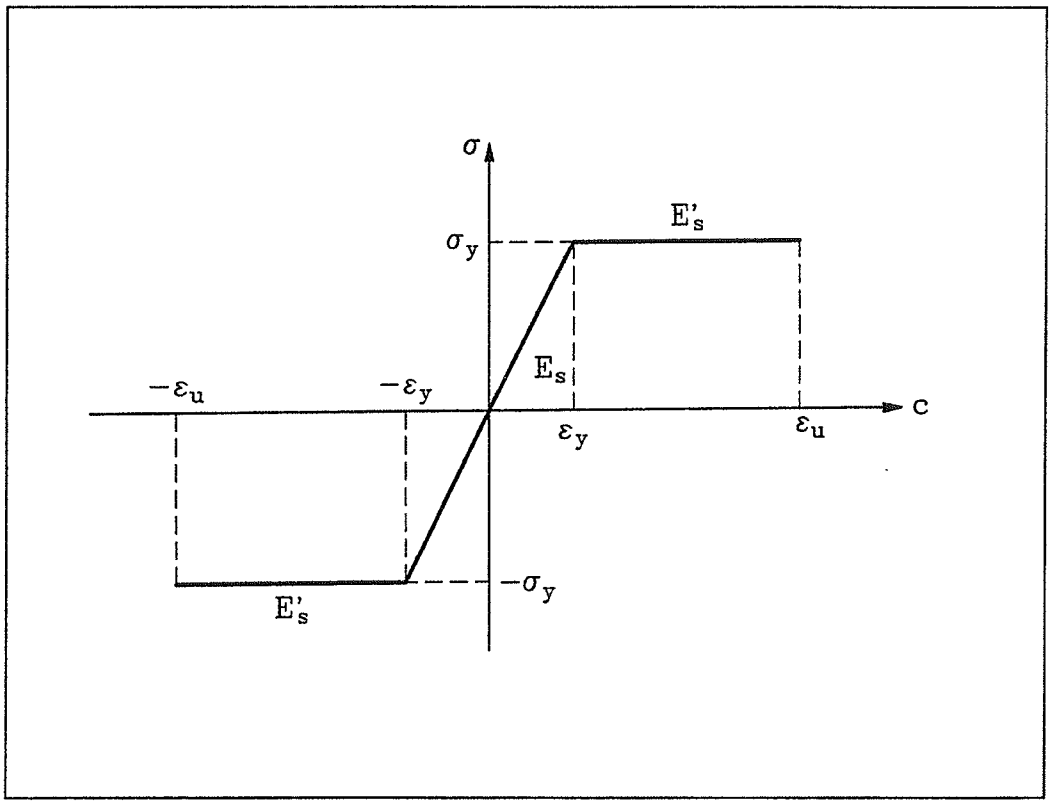

Figure 4.1: Stress/strain diagram for rebars.

5.0 BOND AND SLIP BETWEEN CONCRETE AND REBARS

The traditional effects regarding bond and slip between concrete and rebars have not been included. The effect of compressive strength reduction due to slip of concrete near cracks has been included by the method described in section 3.3.

6.0 RESULTS

As specified in [94.2], results are presented as response time histories, see section 6.1, as horizontal force/displacement relationships, see section 6.2 and as tables and figures summarizing the calculated results for each RUN, see section 6.3.

6.1 Time History Items

In appendix A, figures of the following time history items are plotted for each of the five RUNs:

1) Horizontal acceleration at top of base slab.
2) Horizontal acceleration of center of top slab (calculated and measured).
3) Horizontal displacement of center of top slab (calculated and measured).

6.2 Horizontal Force - Displacement Relationships

In appendix B, figures showing the following force-displacement relationships can be seen:

1) Horizontal force - horizontal displacement of top slab.
2) Horizontal force - vertical relative displacement of right flange.
3) Horizontal force - vertical relative displacement of left flange.

6.3 Summary of Calculated Results

In table 6.1 the following results for each RUN can be found:

1) Initial natural frequency.
2) Maximum response displacement at center of top slab.
3) Maximum response acceleration at center of top slab.

RUN	Initial natural frequency at end of RUN (Hz)	Maximum response displacement (mm)	Maximum response acceleration (m/s^2)
RUN1	13.3	0.29	2.01
RUN2	13.3	0.85	5.61
RUN3	13.0	1.36	6.24
RUN4	10.8	2.90	7.98
RUN5	8.3	10.46	13.91

Table 6.1: Summary of results from dynamic analyses.

In table 6.2, a summary of the calculated results from the static analysis can be seen. In figure 6.1 the locations of the phenomena in table 6.1 are shown (by the corresponding letter).

Phenomena	Horizontal displ. (mm)	Horizontal force (kN)
(a) Flange wall. Initiation point of bending crack.	0.6	475
(b) Web wall. Initiation point of shear crack.	1.3	747
(c) Flange wall vert. rebar. Initiation point of yield.	7.6	1,479
(d) Web wall vert. rebar. Initiation point of yield.	9.0	1,597
(e) Web wall hor. rebar. Initiation point of yield.	16.3	1,909
(f) Crush point	16.3	1,909
Maximum load	16.3	1,909

Table 6.2: Summary of calculated results for top slab (static analysis).

In figure 6.2-3 the appearance of concrete cracks at 2/3 of the maximum load and at the maximum load, resp., can be seen. The line style and thickness of each crack indicate the size of the tensile strain perpendicular to the crack. (Dotted lines indicate tensile strains < dashed lines < full lines < full, thick lines.)

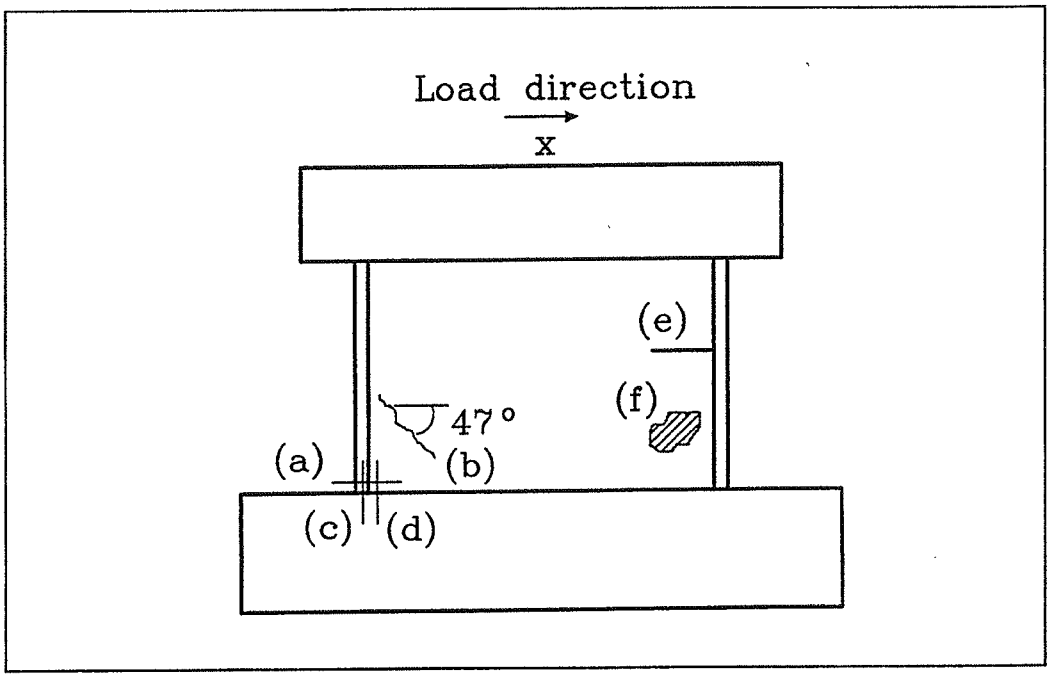

Figure 6.1: Location of phenomena.

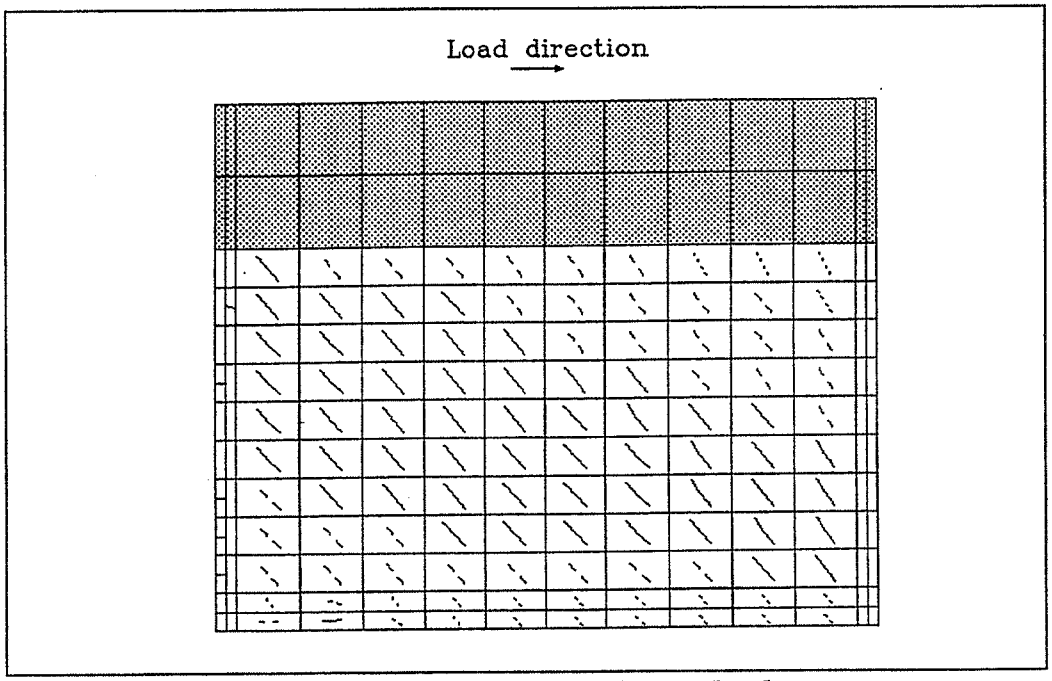

Figure 6.2: Crack formation at 2/3 of maximum load.

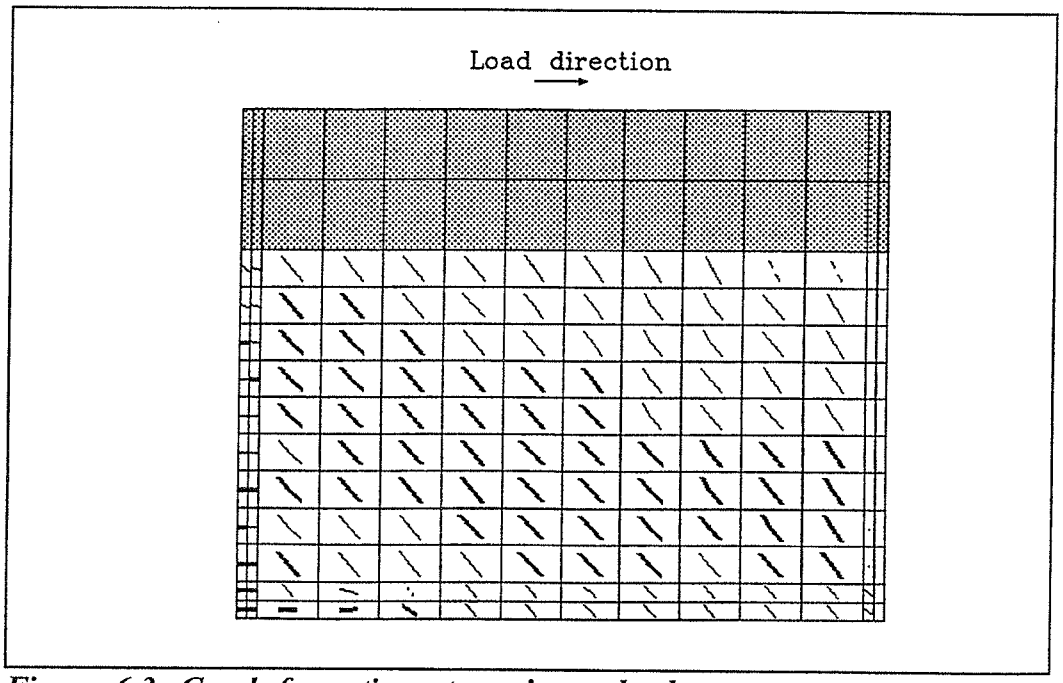

Figure 6.3: Crack formation at maximum load.

6.4 Comparison with Test Results

By comparing the horizontal accelerations and displacements at the top slab, determined from the test and the lumped mass analysis resp., the following items are noted:

1) For RUN1 the correspondence between test and analysis is almost exact. The behaviour in RUN1 is purely elastic.

2) For RUN2 the correspondence is very good for the first 4-5 seconds. After this stage, a discrepancy is present. This indicates that the envelope curve determined from the static analysis is not accurate, at the stage at which most cracking takes place.

3) For RUN3 and RUN4 large non-linearities are present. The correspondence between test and analysis results is very good.

4) For RUN5 the correspondence between test and analysis results is very good for the first three seconds of the analysis. However, after this stage some discrepancies are present. In contrast to the actual test results, the analysis does not predict collapse of the structure in RUN5. Apparently, the load carrying capacity, determined by the static analysis is too high towards the end of the analysis. This indicates that the load/displacement curve, determined from the static FEM analysis, is inaccurate towards the end of the analysis or that it should be reduced when used as an envelope curve for cyclic, large deformation loading. By increasing the ground accelerations by 15%, collapse was predicted by the analysis.

In figure 6.4, the relation between maximum inertial force and maximum displacement for each RUN is shown. The correspondence is seen to be excellent.

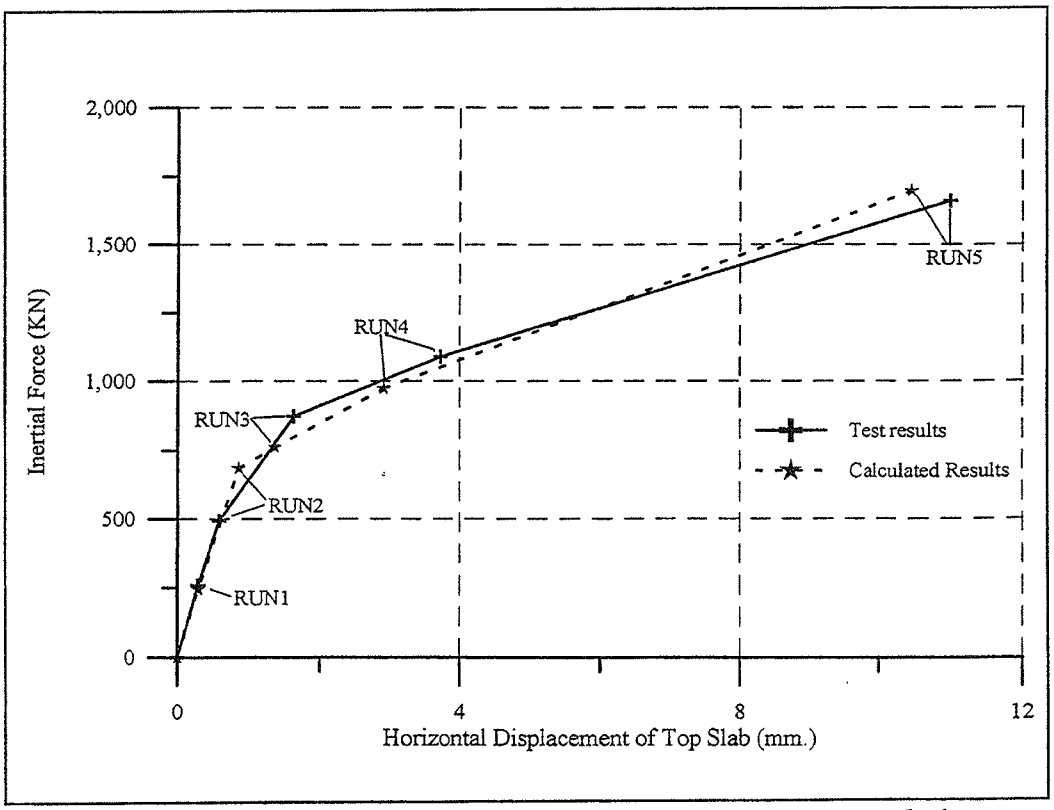

Figure 6.4: Maximum inertial force/maximum displacement relationships.

For this type of problem, the proposed solution method is excellent. For systems of shear walls, in [96.2], a method that introduces only one degree of freedom for each shear wall and in which the non-linear behaviour of each shear wall is determined from an independent load/displacement envelope curve, is presented.

7.0 CONCLUSION

In this report, the non-linear behaviour of a shear wall, subjected to five earthquakes of increasing magnitude (RUN1-5), each of a duration of 12 seconds, is examined. The shear wall is represented by a one degree of freedom model and analysed by a lumped mass analysis. The envelope curve used is non-linear and based on a non-linear static FEM analysis.

The non-linear static FEM analysis is based on an original code described in section 3 and more thoroughly in ref. /96.1/.

The total CPU time for the static analysis was 15 minutes. The total CPU time for the 5 non-linear dynamic analyses was approximately 15 seconds. All analyses were performed on a 586/100 MHz PC with 8 MB RAM.

The correspondence between test and analysis results is excellent, the simplifications and the CPU time of the analyses taken into account. Especially the correspondence between maximum displacement and maximum acceleration, for each of the 5 RUNs, is good. In contrast to the test results, the analysis does not predict collapse of the shear wall in RUN5. This is probably due to an overestimation of the ultimate load by the envelope curve. By increasing the amplitudes of RUN5 by 15%, collapse was predicted by the analysis.

It can be concluded that the model proposed is excellent for determining the dynamic behaviour of a shear wall with a large concentrated mass.

REFERENCES

[71.1]: Goto, Y.: "*Cracks formed in Concrete around Deformed Tension Bars*", Journal of American Concrete Institute, Vol. 68, no. 4., April, 1971

[75.1]: Clough, Ray W. and Penzien, Joseph: "*Dynamics of Structures*", McGraw-Hill Book, Inc., United States of America, 1975

[80.1]: Agarwal, Bhagwan D. and Broutman, Lawrence J.: "*Analysis and Performance of Fiber Composites*", John Wiley & Sons, Inc., Canada, 1980

[82.1]: Bathe, Klaus-Jürgen: "*Finite Element Procedures in Engineering Analysis*", Prentice-Hall, Inc., Englewood Cliffs, New Jersey, 1982

[84.1]: Nielsen, M.P.: "*Limit Analysis and Concrete Plasticity*", Prentice-Hall, Inc., Englewood Cliffs, New Jersey, 1984

[90.1]: Olsen, David Holkmann and Nielsen, M.P.: "*Ny teori til bestemmelse af revneafstande og revnevidder i betonkonstruktioner*" (New Theory for Determining Crack Distances and Crack Widths in Concrete Structures), R254, Department of Structural Engineering, Technical University of Denmark, 1990

[92.1]: Dahl, Kaare K.B.: "*Uniaxial Stress-Strain Curves for Normal and High Strength Concrete*", High Performance Concretes in the 90'es - Report 7.6, Department of Structural Mechanics, Technical University of Denmark, February, 1992

[94.1]: "*PROPOSAL of Seismic Shear Wall ISP on NUPEC's Seismic Ultimate Reponse Test*", Committee on the Safety of Nuclear Installations OECD Nuclear Energy Agency and Nuclear Power Engineering Corporation (JAPAN) Seismic Engineering Center, March, 1994

[94.2]: "*Specification Report of Seismic Shear Wall ISP on NUPEC's Seismic Ultimate Dynamic Reponse Test*", Committee on the Safety of Nuclear Installations OECD Nuclear Energy Agency and Nuclear Power Engineering Corporation (JAPAN) Seismic Engineering Center, September, 1994

[94.3]: Jagd, Lars and Christoffersen, Jens and Nielsen, M.P.: "*The HOTCH-POTCH Disk Element - Finite Element for Analysis of Reinforced Concrete Disks*", R317, Department of Structural Engineering, Technical University of Denmark, 1994.

[94.4]: Zhang, Jin-Ping: "*Strength of Cracked Concrete*", R311, Department of Structural Engineering, Technical University of Denmark, 1994

[96.1]: Jagd, Lars: "*Non-linear FEM Analysis of 2D Concrete Structures*", Ph.D. thesis, Department of Structural Engineering and Materials, Technical University of Denmark, 1996 (Pending)

[96.2]: Helgason, Benedikt: "*Dynamiske beregninger af store systemer*" (Dynamic Analyses of Large Systems), Master thesis, Department of Structural Engineering and Materials, Technical University of Denmark, 1996

APPENDIX A - Time History Items

In this appendix, the following figures are included:

A.1: RUN1 - Accelerations at top of base slab (input data).
A.2: RUN1 - Accelerations at center of top slab (calculated).
A.3: RUN1 - Accelerations at center of top slab (measured).
A.4: RUN1 - Displacements at center of top slab (calculated).
A.5: RUN1 - Displacements at center of top slab (measured).

A.6: RUN2 - Accelerations at top of base slab (input data).
A.7: RUN2 - Accelerations at center of top slab (calculated).
A.8: RUN2 - Accelerations at center of top slab (measured).
A.9: RUN2 - Displacements at center of top slab (calculated).
A.10: RUN2 - Displacements at center of top slab (measured).

A.11: RUN3 - Accelerations at top of base slab (input data).
A.12: RUN3 - Accelerations at center of top slab (calculated).
A.13: RUN3 - Accelerations at center of top slab (measured).
A.14: RUN3 - Displacements at center of top slab (calculated).
A.15: RUN3 - Displacements at center of top slab (measured).

A.16: RUN4 - Accelerations at top of base slab (input data).
A.17: RUN4 - Accelerations at center of top slab (calculated).
A.18: RUN4 - Accelerations at center of top slab (measured).
A.19: RUN4 - Displacements at center of top slab (calculated).
A.20: RUN4 - Displacements at center of top slab (measured).

A.21: RUN5 - Accelerations at top of base slab (input data).
A.22: RUN5 - Accelerations at center of top slab (calculated).
A.23: RUN5 - Accelerations at center of top slab (measured).
A.24: RUN5 - Displacements at center of top slab (calculated).
A.25: RUN5 - Displacements at center of top slab (measured).

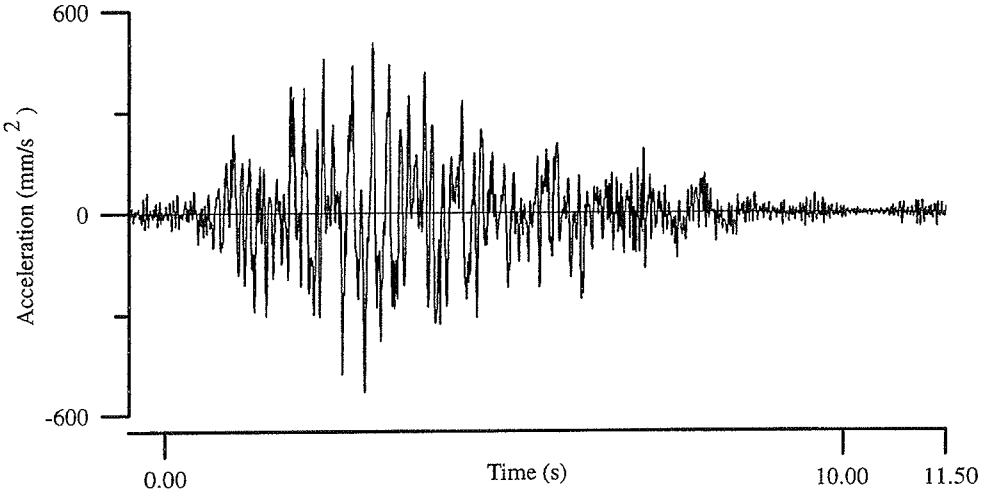

Figure A.1: RUN1 - Accelerations at top of base slab (input data).

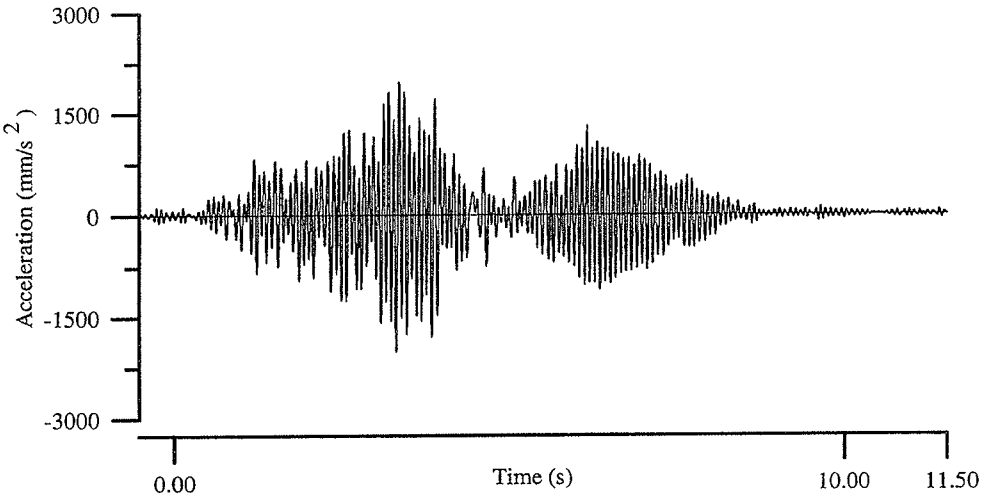

Figure A.2: RUN1 - Accelerations at center of top slab (calculated).

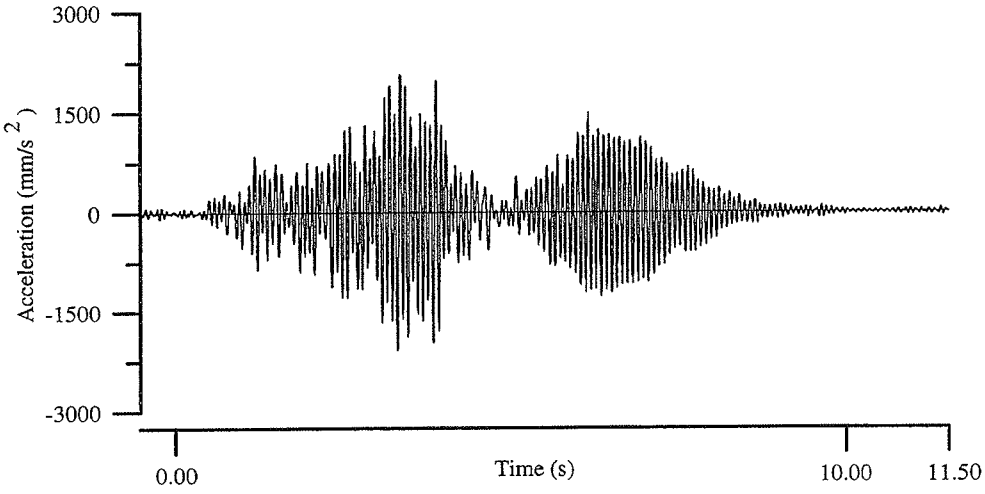

Figure A.3: RUN1 - Accelerations at center of top slab (measured).

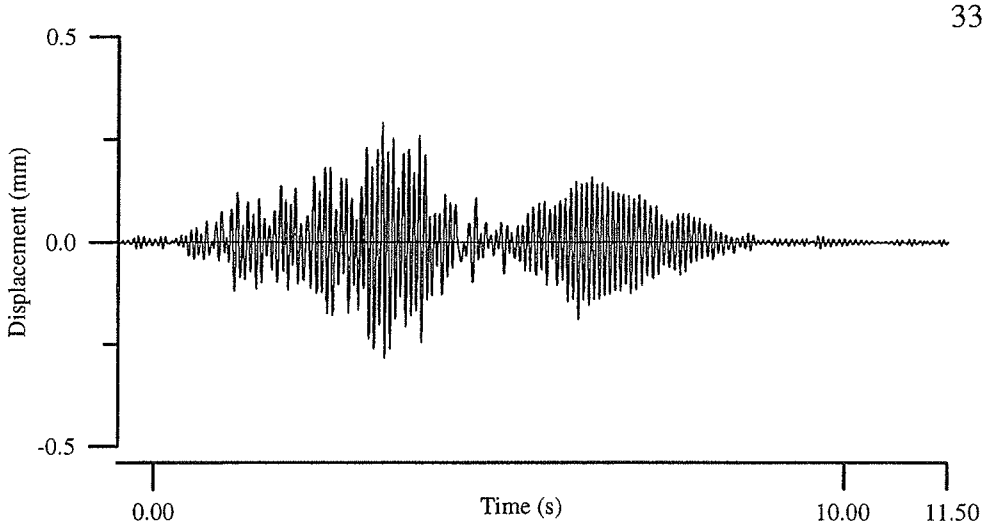

Figure A.4: RUN1 - Displacements at center of top slab (calculated).

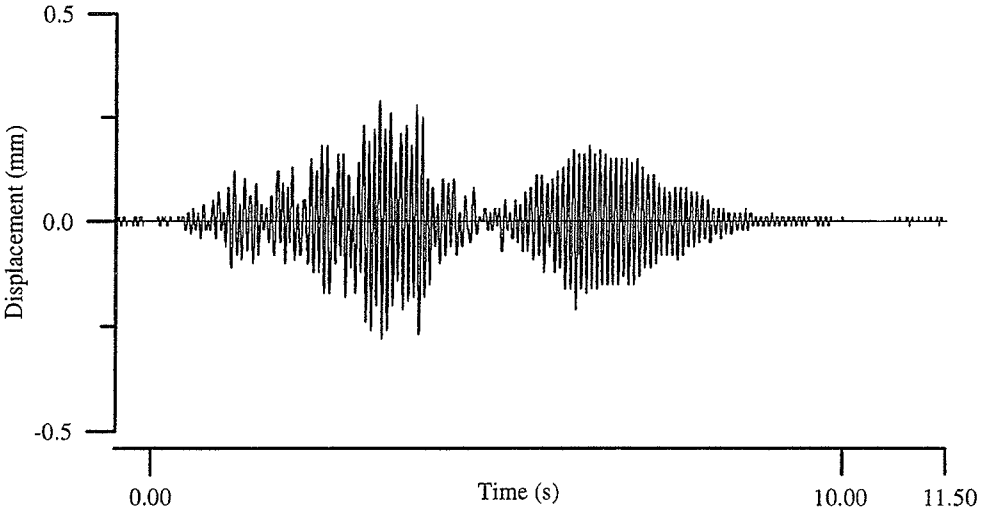

Figure A.5: RUN1 - Displacements at center of top slab (measured).

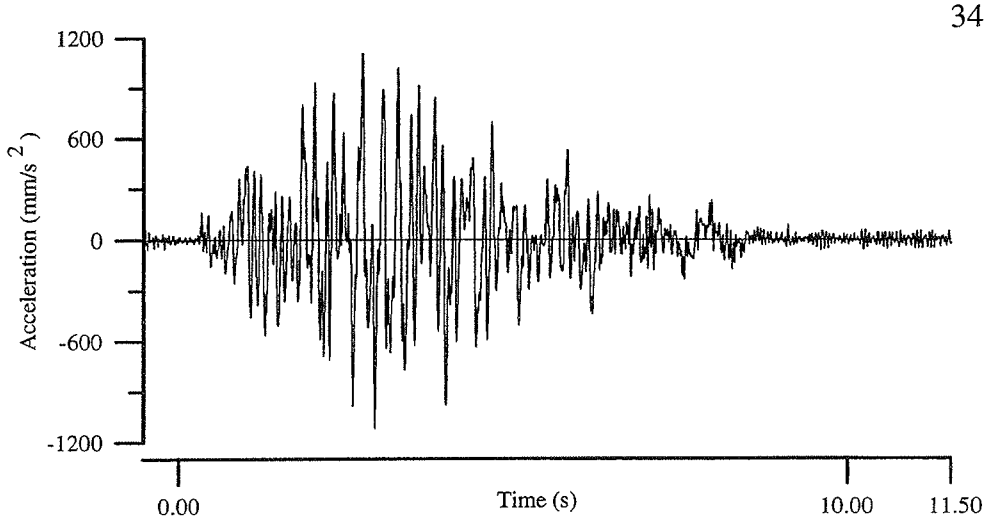

Figure A.6: RUN2 - Accelerations at top of base slab (input data).

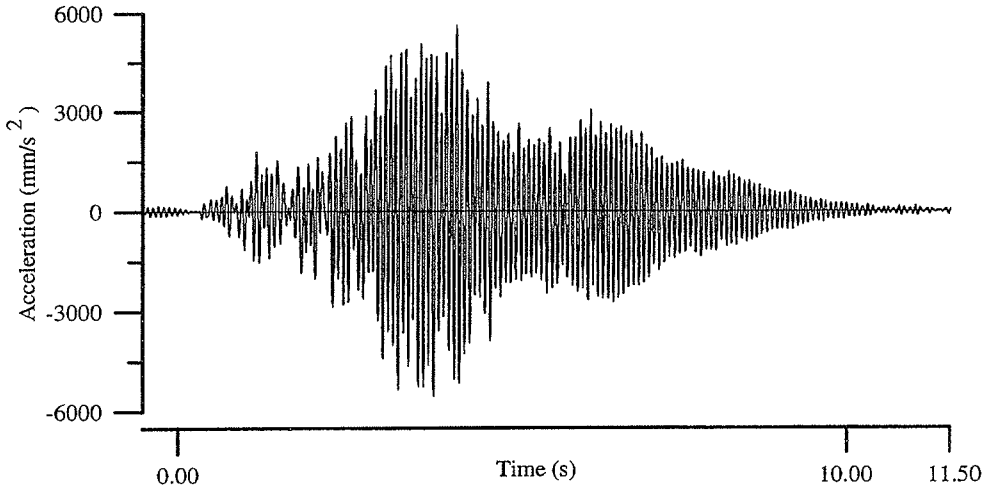

Figure A.7: RUN2 - Accelerations at center of top slab (calculated).

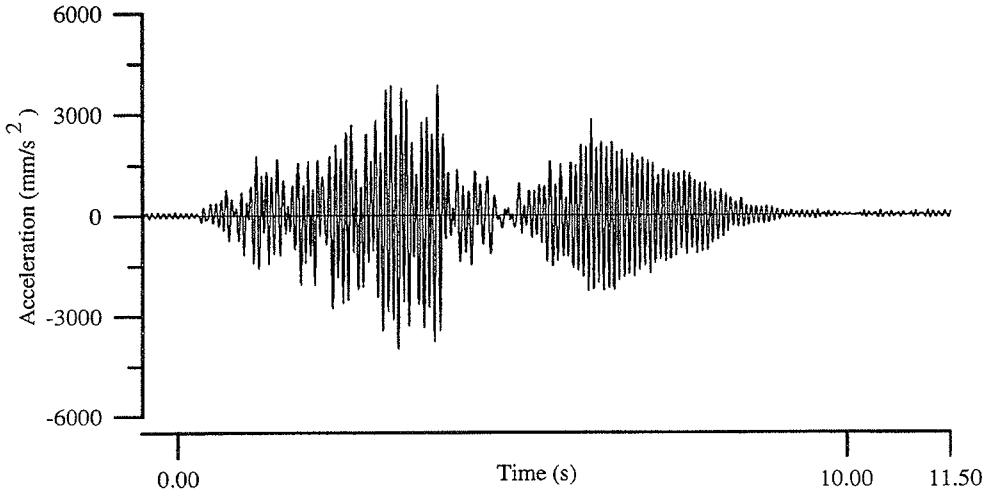

Figure A.8: RUN2 - Accelerations at center of top slab (measured).

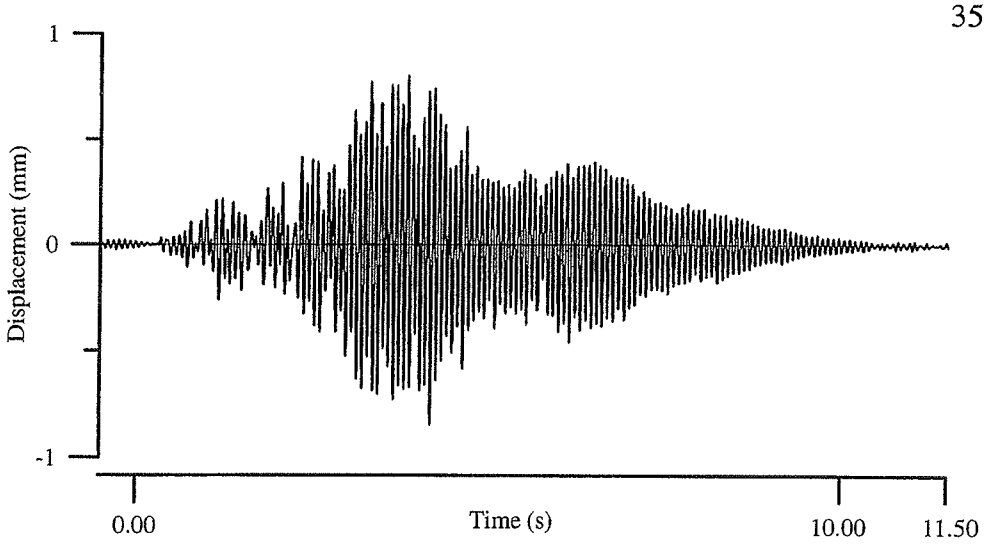

Figure A.9: RUN2 - Displacements at center of top slab (calculated).

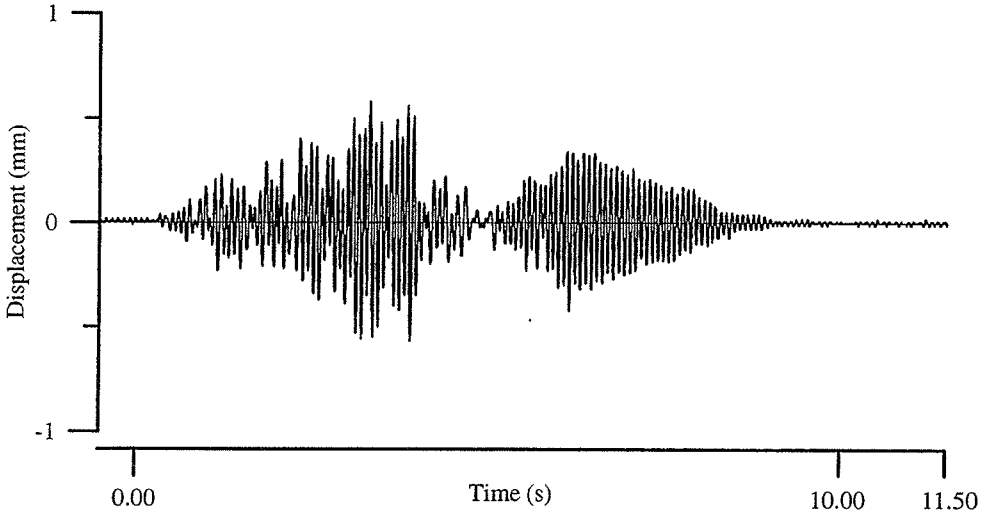

Figure A.10: RUN2 - Displacements at center of top slab (measured).

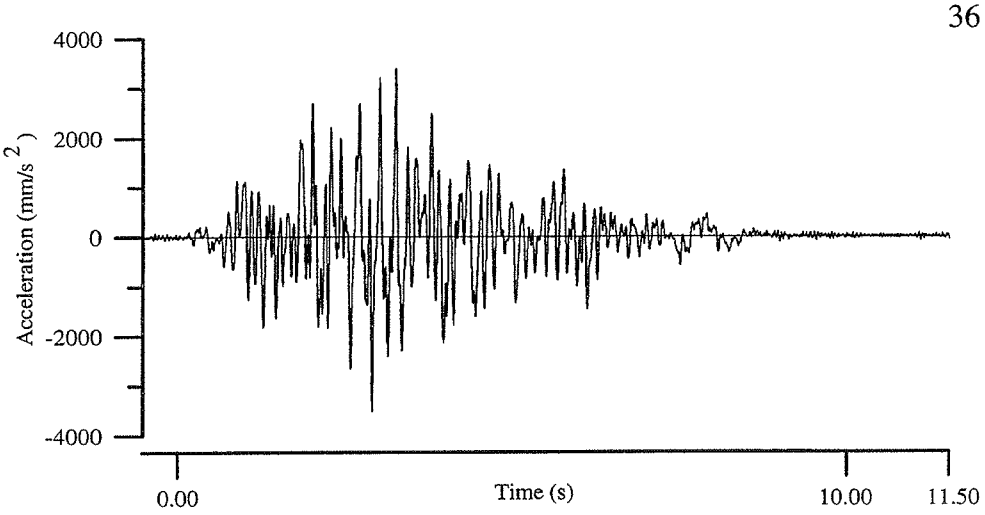

Figure A.11: RUN3 - Accelerations at top of base slab (input data).

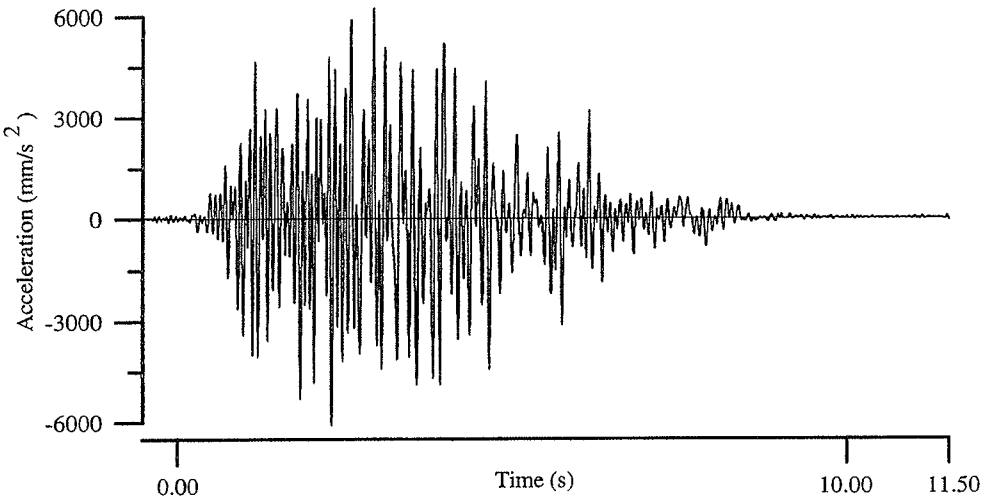

Figure A.12: RUN3 - Accelerations at center of top slab (calculated).

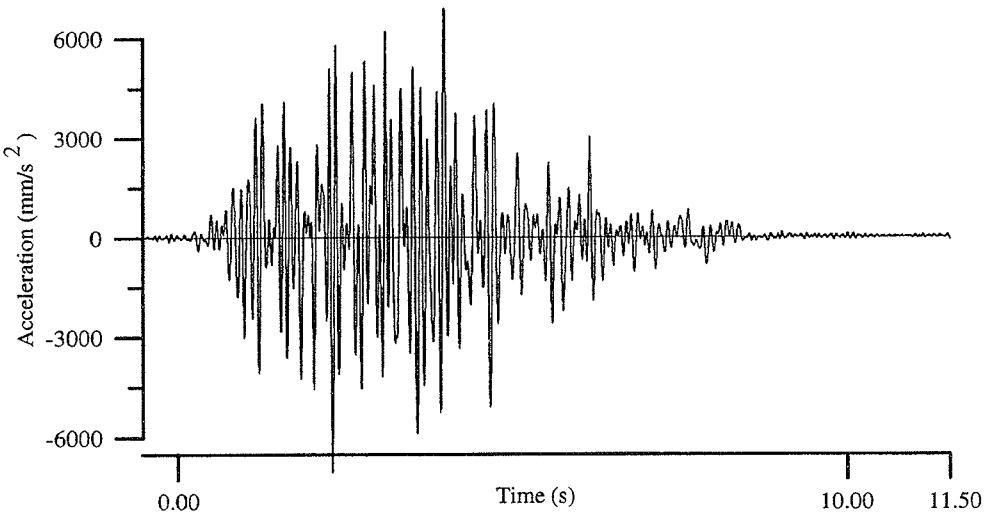

Figure A.13: RUN3 - Accelerations at center of top slab (measured).

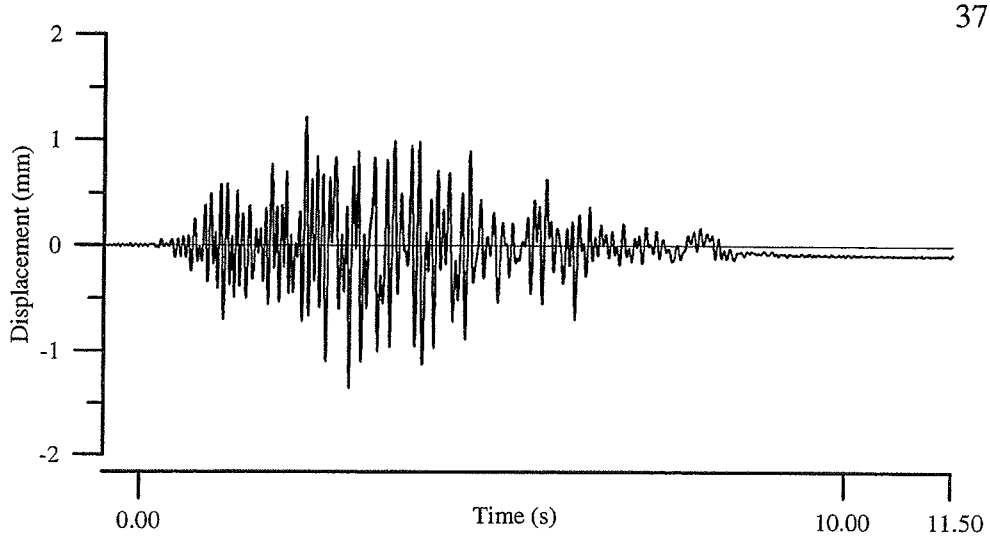

Figure A.14: RUN3 - Displacements at center of top slab (calculated).

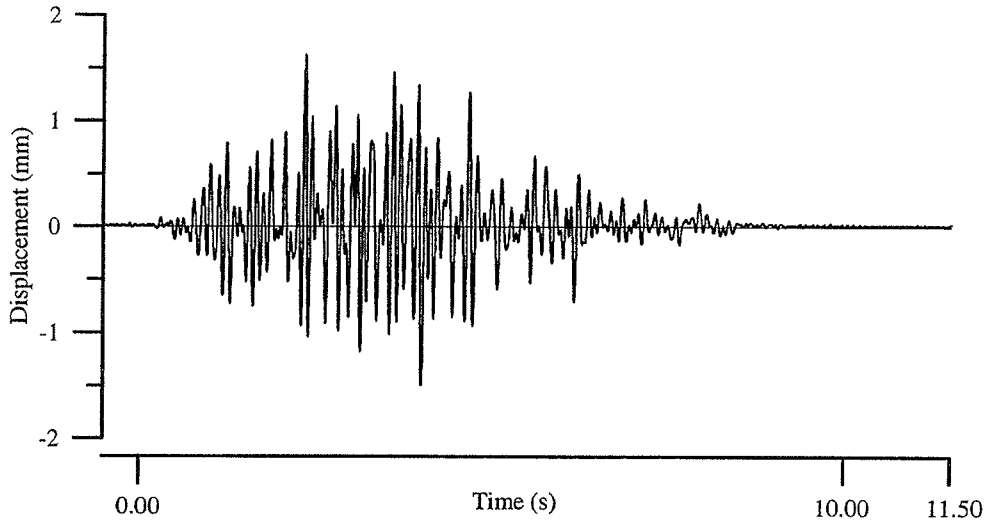

Figure A.15: RUN3 - Displacements at center of top slab (measured).

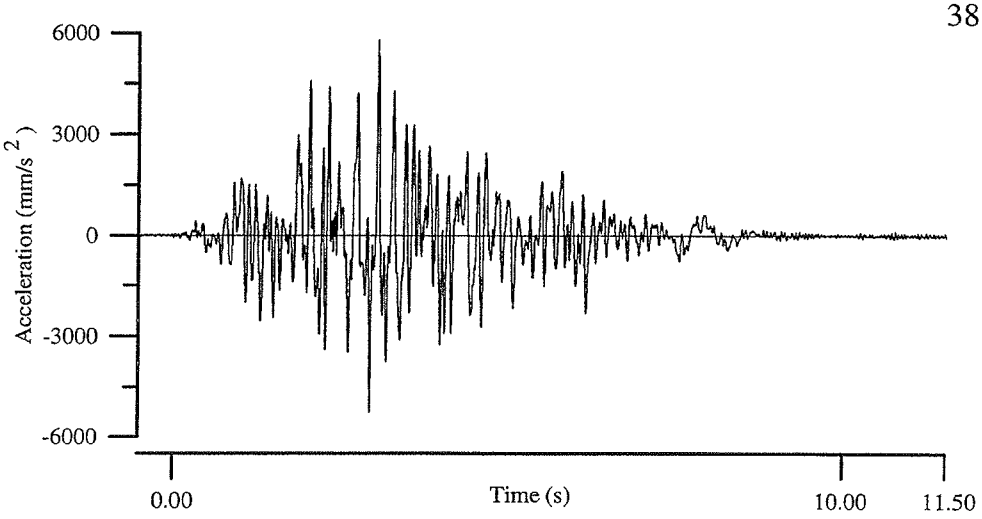

Figure A.16: RUN4 - Accelerations at top of base slab (input data).

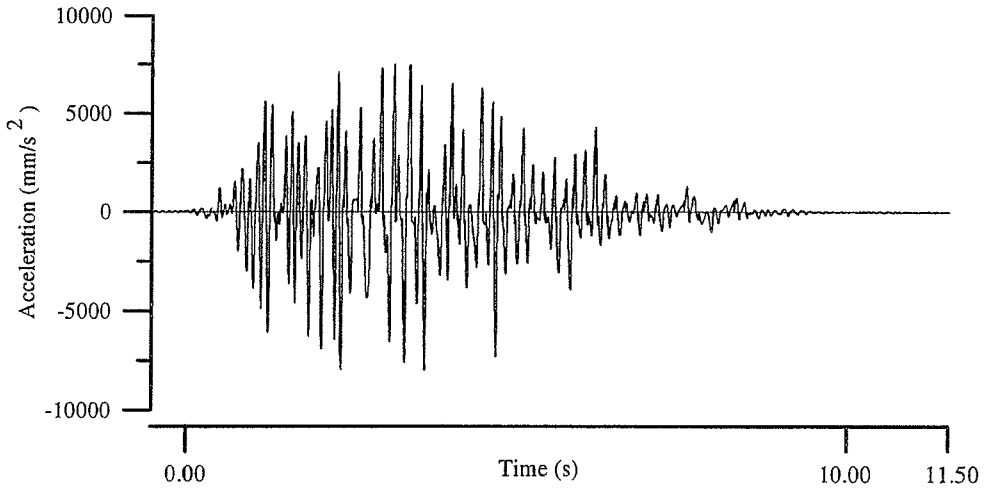

Figure A.17: RUN4 - Accelerations at center of top slab (calculated).

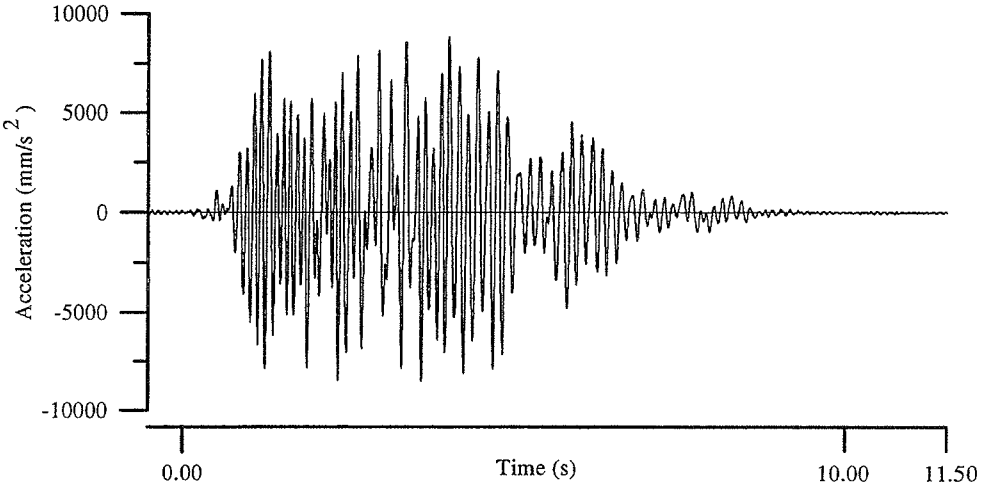

Figure A.18: RUN4 - Accelerations at center of top slab (measured).

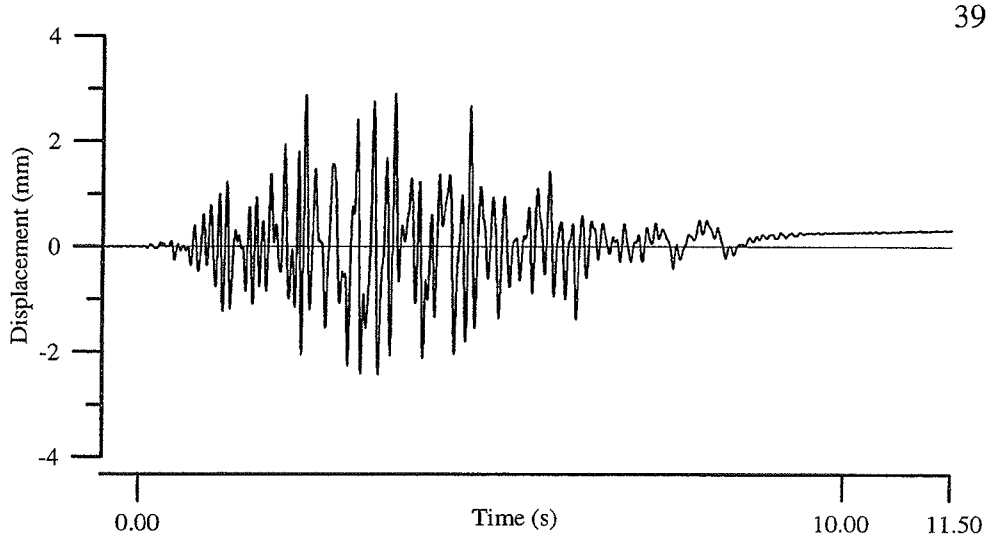

Figure A.19: RUN4 - Displacements at center of top slab (calculated).

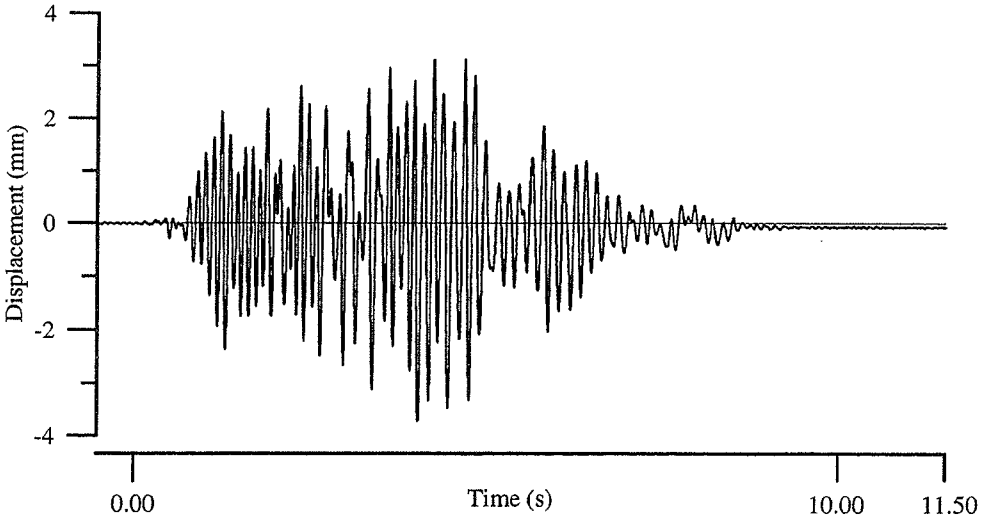

Figure A.20: RUN4 - Displacements at center of top slab (measured).

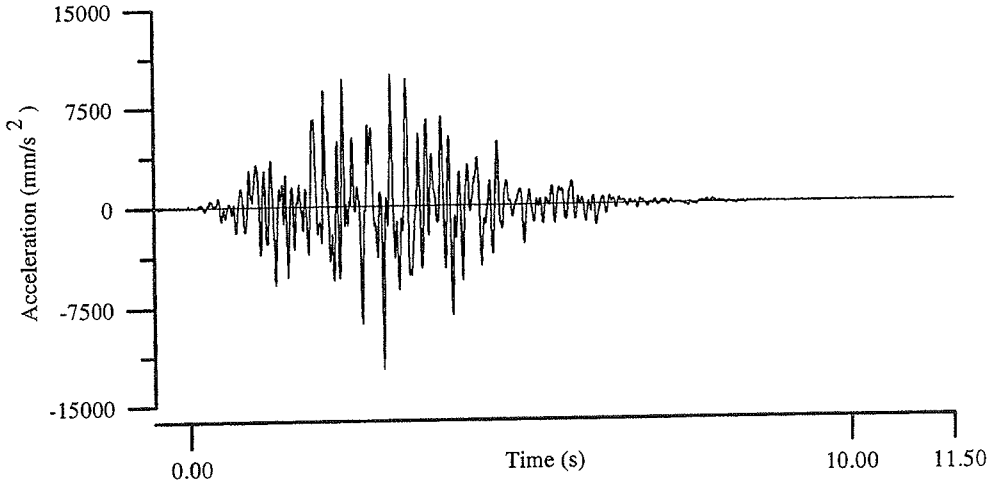

Figure A.21: RUN5 - Accelerations at top of base slab (input data).

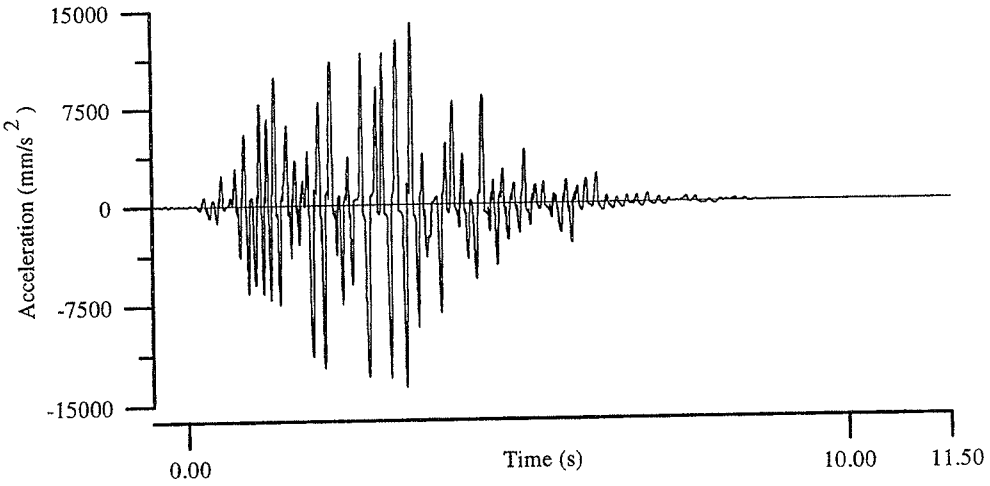

Figure A.22: RUN5 - Accelerations at center of top slab (calculated).

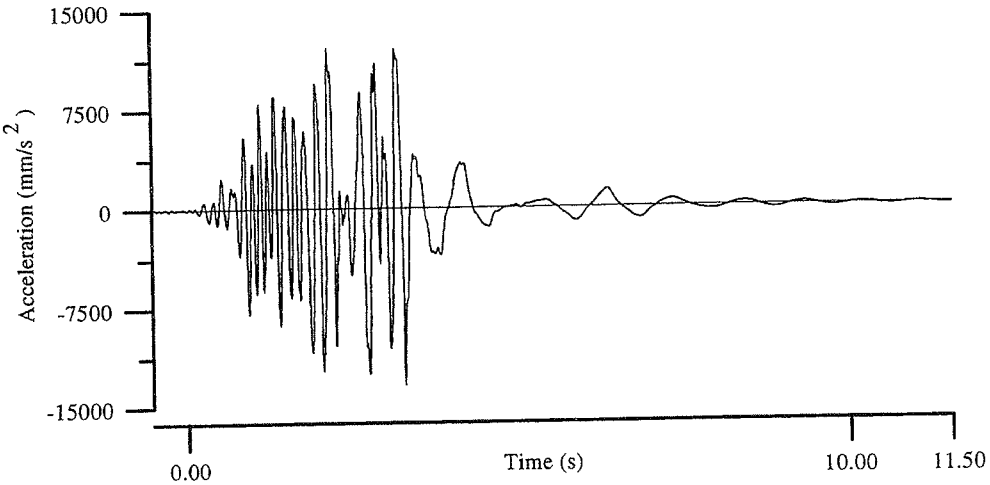

Figure A.23: RUN5 - Accelerations at center of top slab (measured).

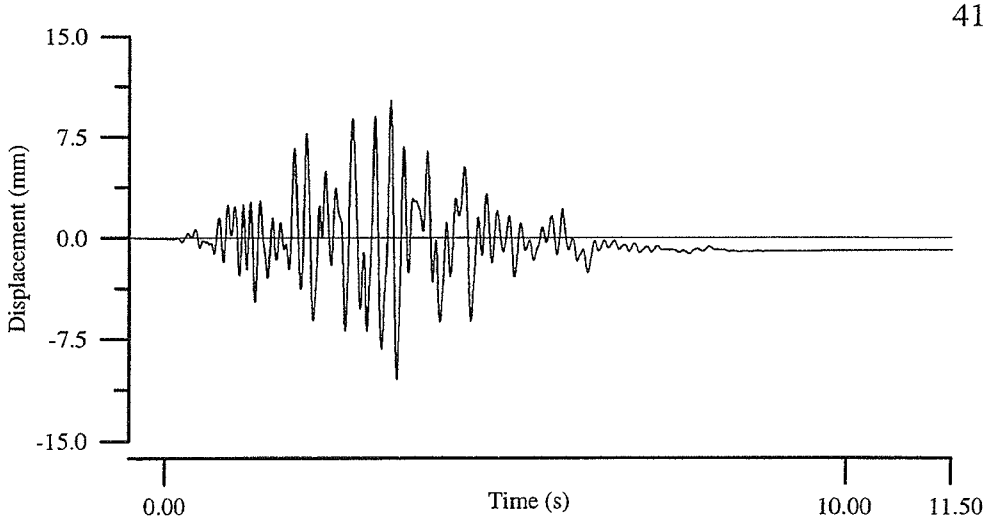

Figure A.24: RUN5 - Displacements at center of top slab (calculated).

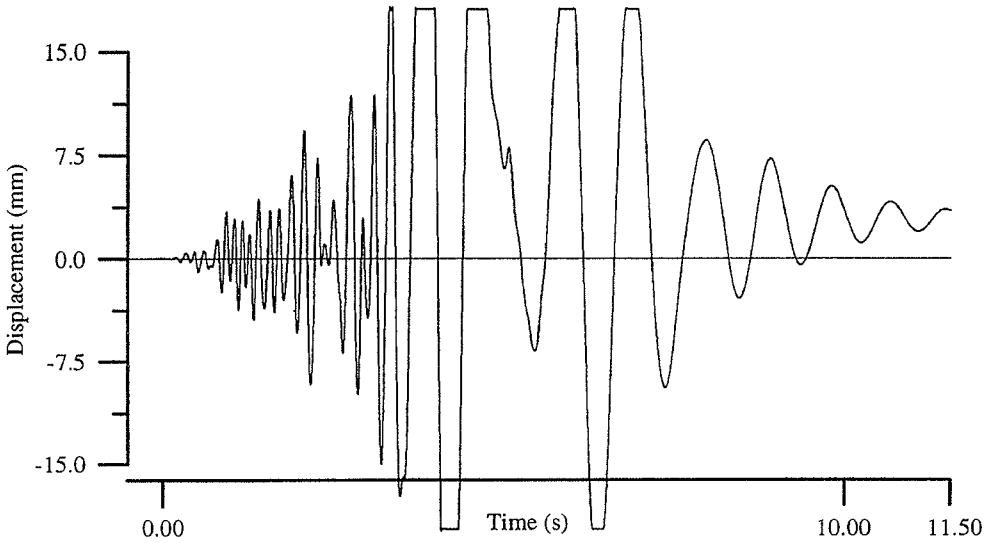

Figure A.25: RUN5 - Displacements at center of top slab (measured).

APPENDIX B - Force / Displacement Relationships

In figure B.1, the horizontal force / horizontal displacement relationship is shown.

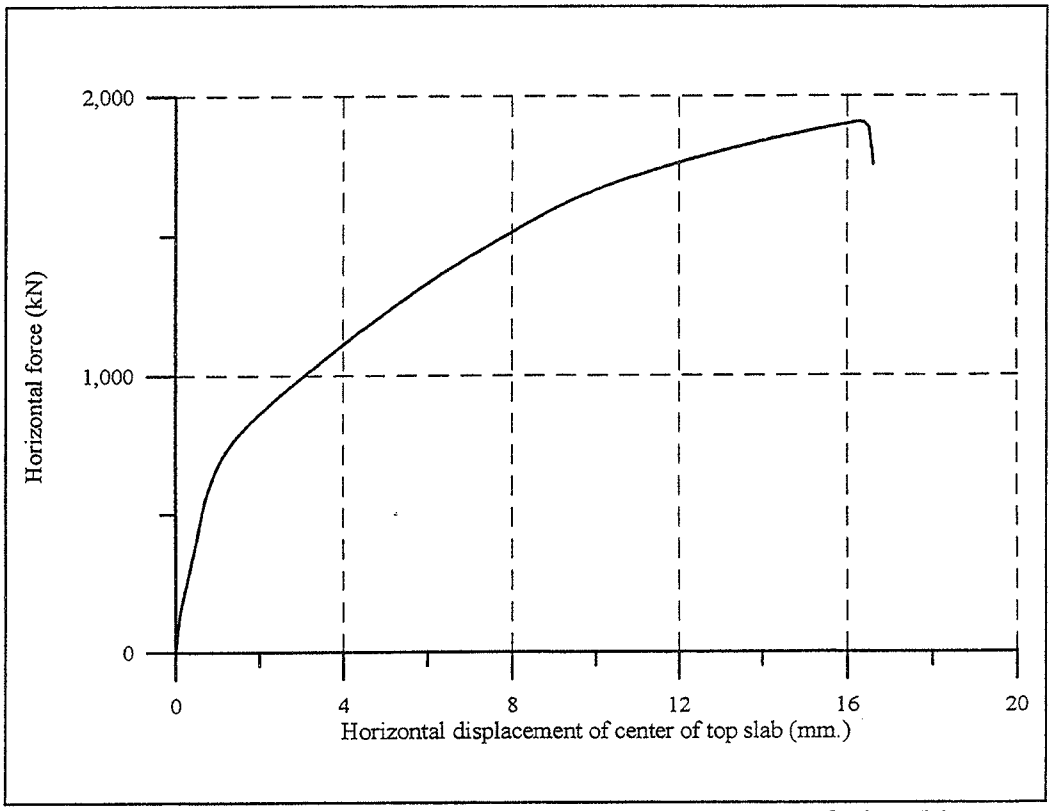

Figure B.1: Horizontal force / horizontal displacement relationship.

In figure B.2, the horizontal force / vertical displacement of right flange relationship is shown.

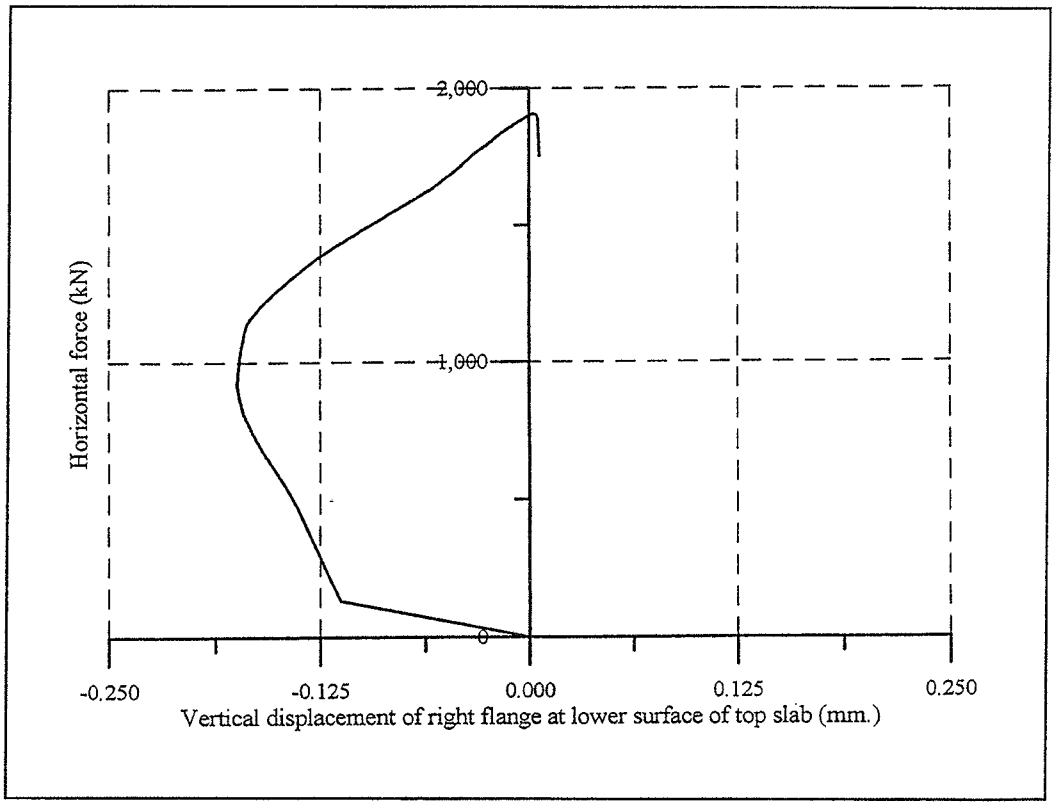

Figure B.2: Horizontal force / vertical displacement of right flange relationship.

In figure B.3, the horizontal force / vertical displacement of left flange relationship is shown.

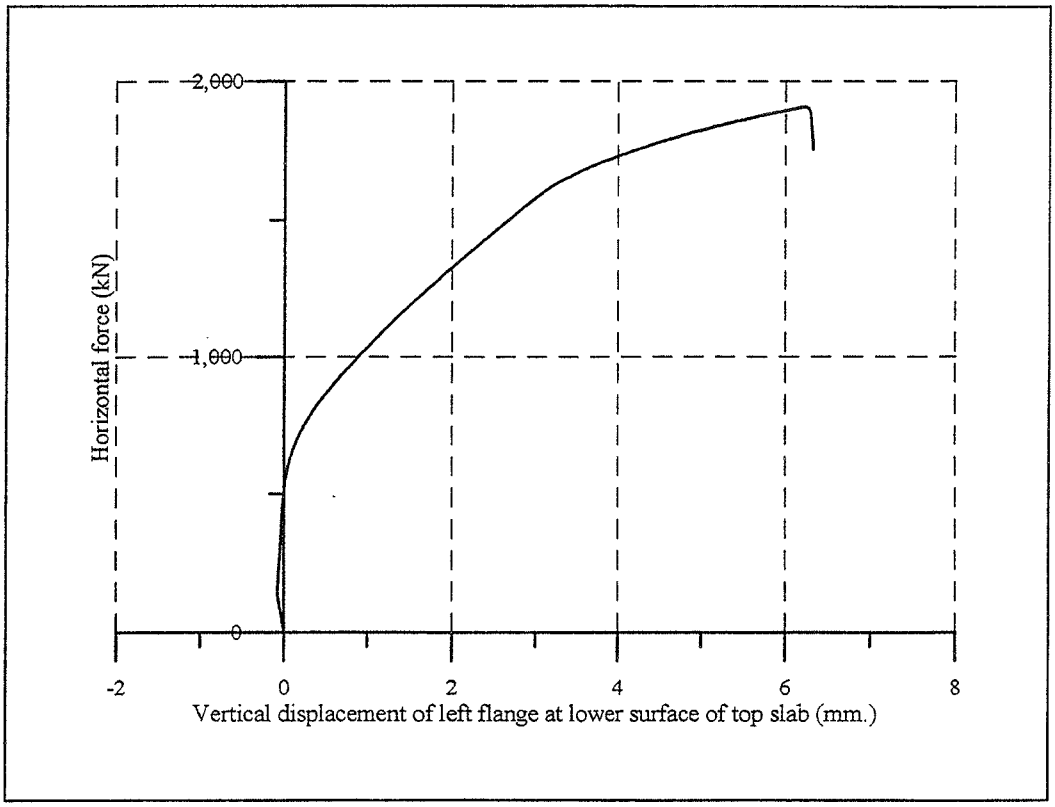

Figure B.3: Horizontal force / vertical displacement of left flange relationship.